

LAPPEENRANTA UNIVERSITY OF TECHNOLOGY  
LUT School of Energy Systems  
Master's Programme in Energy Systems

*Setareh Nakhostin*

**NUMERICAL INVESTIGATION OF HEAT TRANSFER IN THE NEAR-CRITICAL  
POINT APPLICATIONS**

Examiners: Associate Professor Teemu Turunen-Saaresti  
M. Sc. (Tech) Alireza Ameli

## **ABSTRACT**

Lappeenranta University of Technology  
LUT School of Energy Systems  
Master's Programme in Energy Systems

Setareh Nakhostin

### **Numerical Investigation of Heat transfer in the Near- Critical Point Applications**

Master's thesis

2018

73 pages, 26 figures and 4 tables

Examiners: Associate Professor Teemu Turunen-Saaresti

M. Sc. Alireza Ameli

Keywords:  $\text{SCO}_2$  Brayton cycle, PCHE, friction factor correlation, supercritical fluid

In recent years, employing  $\text{CO}_2$  in supercritical Brayton cycle in industry is under research and development due to its enormous advantages specifically high thermal efficiency of cycle at operating condition with relative lower turbine inlet temperature compared to other cycles. Uncommon behavior in fluid properties near the critical point can cause uncertain numerical simulation, which should be investigated through optimizing design parameters such as flow characteristics and boundary layer behavior. In present study, a large horizontal heated pipe at different experimental conditions such as mass flow rates, heat fluxes and boundary conditions have been studied. The numerical simulation has been examined with different turbulence models and the best approach based on comparing CFD and given experimental results was selected. The trend of friction factor coefficient in heated pipe investigated and compared to other well-known friction factor correlations. Results showed that part of selected friction factor correlations have the best match with CFD results and some of them cannot be applied.

## **Dedication**

**This master thesis is dedicated to my parents, specifically my dad,**

**For your patience, full support and informative guidance.**

## **ACKNOWLEDGEMENT**

I would like to give appreciative thanks to my first adviser associate Professor Teemu Turunen-Saaresti, for his neat comments to enhance my work.

I would like to express my special thanks to my second adviser Doctoral candidate, Alireza Ameli for his constant inspiration that motivated me to choose this topic and his instructive guide and continues encouragement to carry out my master thesis.

I would also like to thank Professor Esa K. Vakkilainen to trust me and gave me the chance for studying energy system engineering.

Setareh Nakhostin

October 23, 2018

Lappeenranta, Finland

## TABLE OF CONTENTS

ACKNOWLEDGEMENT .....	3
LIST OF TABLES .....	6
LIST OF FIGURES .....	7
NOMENCLATURE .....	9
1 INTRODUCTION .....	9
1.1 Objectives.....	10
1.2 Brayton cycle vs. Rankine cycle .....	11
1.3 Advantages of CO <sub>2</sub> as a working fluid in supercritical phase.....	12
1.4 SCO <sub>2</sub> Brayton cycle- Advantages .....	13
2 HEAT TRANSFER AT CO <sub>2</sub> PHASE .....	15
2.1 Thermophysical properties at SCO <sub>2</sub> phase.....	16
3 COMPARING REAL GAS AND IDEAL GAS THERMODYNAMIC .....	17
3.1 Van der waals.....	18
3.2 Cubic equation of states .....	18
3.2.1 Redlich Kwong model.....	19
3.2.2 Standard Redlich Kwong model.....	19
3.2.3 Peng Robinson model.....	19
3.2.4 Span Wagner Model .....	20
3.3 Compressibility factor.....	21
4 TYPES OF HEAT EXCHANGERS.....	22
4.1 Fin type heat exchanger .....	23
4.2 Shell and tube heat exchanger:.....	23
4.3 Compact heat exchanger .....	24
4.3.1 Printed circuit heat exchanger (PCHE) .....	25
5 PARAMETERS AFFECT FLOWAND HEAT TRANSFER IN SCO <sub>2</sub> HEAT EXCHANGER.....	28
5.1 Tube diameter.....	28
5.2 Channel characteristics.....	29
5.3 Surface heat flux .....	29
5.4 Inlet pressure .....	30

5.5	Inlet temperature .....	31
5.6	Inlet mass flux .....	32
5.7	Pressure drop .....	32
6	FRICITION FACTOR .....	33
6.1	Past studies .....	34
6.2	Boundary layers and universal law of wall .....	35
6.3	Turbulence models .....	38
7	CURRENT MODEL: COMPUTATIONAL FACT .....	39
7.1	Governing equations .....	39
7.2	Geometry, mesh grid and boundary conditions .....	40
7.3	Numerical approach .....	43
8	COMPARISON AND VALIDATION OF NUMERICAL MODEL WITH EXPERIMENTAL DATA .....	44
9	RESULTS AND DISCUSSION .....	45
9.1	wall temperature distribution .....	45
9.2	Heat transfer coefficient .....	46
9.3	Friction factor coefficient .....	48
10	VALIDATION OF DIFFERENT FRICTION FACTOR CORRELATIONS AGAINST CFD RESULTS .....	50
11	VELOCITY AND DENSITY CONTOURS .....	53
12	CONCLUSION .....	57
12.1	Summery of investigated model .....	57
12.2	Summary of Results and validations .....	58
12.3	Further work recommendation .....	59
	REFERENCES .....	60
	APPENDIX: .....	68
	Test 1.1 .....	68
	Test 2.1 .....	70
	Test 3.1 .....	72

## **LIST OF TABLES**

<b>No.</b>	<b>Title</b>	<b>Page</b>
1	Critical conditions for different fluids	12
2	Experimental conditions	42
3	Comparison of average friction factor in heating wall with adiabatic wall	49
4	List of friction factor correlations used in validation	50

## LIST OF FIGURES

No.	Title	Page
1	Comparing thermal efficiencies of different conversion systems	11
2	Recompression Brayton cycle	14
3	Temperature-entropy diagram of RBC	15
4	Thermophysical properties of $\text{SCO}_2$ near critical point with respect to temperature at different pressures	17
5	Comparing compressibility factors for different gases	22
6	Fin type heat exchanger configurations	23
7	Shell and tube heat exchanger configuration	24
8	Compact heat exchanger configuration	24
9	PCHE components during manufacturing	27
10	Different PCHE channels: straight, zigzag, S shaped and airfoil	27
11	Velocity and thermal gradient	36
12	Velocity distribution in boundary layers	37
13	Cross section of mesh grid used in simulation	41
14	Mesh dependency test for CFD case 1.1 with coarse and fine mesh	41
15	Schematic of numerical model	41
16	Operating range of investigated heat exchanger	42
17	Convergence results of CFD cases	44
18	Validation of wall temperature distribution simulated by different turbulence model against Adebiyi and Hall experimental results	45
19	Temperature distribution of numerical results based on SST turbulence model against experimental results in four tests conditions	46

20	Heat transfer distribution of numerical results based on SST turbulence model based on four tests conditions	47
21	Friction factor coefficient of numerical results based on SST model in four tests conditions	49
22	Validation of numerical results of friction factor coefficient (top/Bottom wall) against some friction factor correlations	52
23	Validation of numerical results of friction factor coefficient (Top/Bottom average) against best match friction factor correlations	53
24	Velocity contour of one cross section	54
25	Flow domain and cross sections conditions	54
26	Velocity and density contours of numerical results in 1.2 test condition	56

## NOMENCLATURE

$A$	Helmholtz energy function [-]
$A_s$	Heat transfer surface area [m <sup>2</sup> ]
$a$	Attraction between particles [-]
$b$	Volume of particles [-]
$C_p$	Specific heat [J/kg K]
$c_v$	Specific volume [-]
$D$	Tube diameter [m]
$D_h$	Hydraulic diameter [m]
$D_w$	Cross diffusion [-]
$f$	Friction factor coefficient [-]
$C_f$	Friction factor coefficient [-]
$G$	Mass flux [kg/m <sup>2</sup> s]
$G_k$	Kinetic energy of turbulence mode [-]
$G_{kw}$	$\omega$ generation [-]
$g$	Acceleration due to gravity [m/s <sup>2</sup> ]
$h$	Convection heat transfer coefficient [W/m <sup>2</sup> °C]
$H$	Enthalp [J/kg]
$j$	Colburn j factor [-]
$k$	Thermal conductivity [W/mK]
$k$	Turbulent kinetic energy [-]
$L$	Length of pipe [m]

$\dot{m}$	Mass flow rate [kg/s]
$N$	Number of thermal units [-]
$N_u$	Nusselt number [-]
$n$	Number of moles [-]
$P$	Pressure [Pa]
$P_c$	Critical pressure [-]
$P_{cr}$	Critical pressure [-]
$P_R$	Reduced pressure [-]
$Pr$	Prandtl number [-]
$\Delta P$	Pressure drop [Pa]
$\dot{Q}_{conv}$	Convection heat transfer rate [Watt]
$q$	heat flux [W/m <sup>2</sup> ]
$R$	Ideal gas constant [-]
$Re$	Reynolds number [-]
$S$	Entropy [-]
$S_k$	User defined source terms [-]
$S_w$	User defined source terms [-]
$T$	Temperature [°C]
$T_s$	Surface temperature [°C]
$T_\infty$	Fluid temperature [°C]
$T_f$	Fluid temperature [°C]
$T_m$	Mean temperature along a tube [°C]

$T_c$	Critical temperature [°C]
$T_{cr}$	Critical temperature [°C]
$T_R$	Reduced temperature [°C]
$T_{out}$	Outlet temperature [°C]
$T_{in}$	Inlet temperature [°C]
$\Delta T_m$	Mean temperature difference [°C]
$t$	Time [s]
$T_w$	Wall temperature [°C]
$T_b$	Bulk temperature [°C]
$u^+$	Dimensionless velocity [-]
$u_r$	Friction velocity [-]
$v$	Velocity [m/s]
$u$	Velocity [m/s]
$V$	Volume [m <sup>3</sup> ]
$V_m$	Molar volume [-]
$v$	Specific volume [-]
$\omega$	Acentric factor [-]
$y^+$	Dimensionless distance to the wall [-]
$Y_k$	k dissipation [-]
$Y_w$	$\omega$ dissipation [-]
$Z$	Compressibility factor [-]

Greek Letters

$\kappa$	Von karman constatnt [-]
$\mu$	Dynamic viscosity [Pa s]
$\mu_t$	Turbulent viscosity [-]
$\tau_w$	Shear stress [-]
$\tau$	Inverse reduced temperature [-]
$\rho$	Density [kg/m <sup>3</sup> ]
$\rho^{VAP}$	Density of vaporization [-]
$\Gamma_k$	k effective diffusivity [-]
$\Gamma_w$	$\omega$ effective diffusivity [-]
$\delta$	Inverse reduced density/ Thickness of boundary layer [-]

#### Subscripts and Superscripts

0	Ideal gas
<i>b</i>	bulk
<i>c/c<sub>r</sub></i>	Critical value
<i>r</i>	Residual behavior of fluid
<i>i</i>	general spatial indicate
<i>in</i>	Inlet
<i>out</i>	Outlet
<i>R</i>	Reduced
<i>w</i>	Wall
<i>VAP</i>	Vaporization
'	Fluctuation

## 1 INTRODUCTION

Today, environmental issues become a threat for ecosystem and organisms, which can be managed through green as well as sustainable technology improvement. In this regard, one of the practical industrial solutions can be replacing conventional cycles by high efficient supercritical Brayton cycle in power plants. Employing supercritical carbon dioxide (SCO<sub>2</sub>) Brayton cycle can be exceedingly beneficial from three general aspects, including: efficiency enhancement, cost and environmental matter.

First, about thermal efficiency enhancement, both best advantages of simple Brayton cycle and Rankine cycle are put together in one cycle (SCO<sub>2</sub> Brayton cycle); meaning, “CO<sub>2</sub> compressed in the region with liquid like density and higher turbine inlet temperature can be utilized with less material issues compared to steam Rankine cycle”( Ahn, et al., 2015).

Second, reducing the cost of energy supply can be achievable through minimizing the component size of thermodynamic cycle. The prerequisite for size reduction approach is choosing the appropriate heat exchanger type. In fact, the design of heat exchanger allows size reduction approach effectively. Therefore, using compact heat exchanger, specifically PCHE would be a neat choice. The employed technology to produce PCHE causes to reduce hydraulic diameter of heat exchanger. It is worth mentioning that, increasing pressure drop in heat exchanger, which has inverse relation with channel hydraulic diameter, decrease the cycle efficiency. Consequently, studying one of the major factors that influences pressure drop, which is friction factor coefficient, is highly considered. Technology improvement in this regard can significantly push the barrier of using PCHE in industry.

Third, about environmental issues, CO<sub>2</sub> has low global warming potential (GWP). Besides, it has significant low (near zero) Ozone depletion potential (ODP), non -toxic/flammable, abundant and inexpensive. According to Dostal, et al. (2004), it is a stable fluid with “relative inertness” (for the temperature range of interest). The unique thermodynamic characteristics of CO<sub>2</sub> near critical point leads to nonlinear behavior, causes effective heat transfer at given operating condition.

## 1.1 Objectives

The aim of this thesis is to clarify understanding of  $\text{SCO}_2$  heat transfer characteristics in horizontal heat exchanger, in particular how friction factor has an impact on heat transfer in specific defined geometry and orientation. In first chapter, different common thermodynamic cycles are compared, followed by  $\text{CO}_2$  characteristic as a working fluid and then the advantages of  $\text{SCO}_2$  Brayton cycle has been discussed. Second chapter mainly relates to sharp behavior of  $\text{SCO}_2$  thermodynamic properties, specifically near critical point. Chapter three is devoted to comparing between the real gas and ideal gas as well as their difference values or behaviors with respect to corresponded equations. In chapter 4, different types of heat exchanger are introduced and the most promising heat exchanger for  $\text{SCO}_2$  Brayton cycle is suggested and explained in details. Moreover, parameters affecting flow and heat transfer in  $\text{SCO}_2$  heat exchanger will be reviewed in chapter 5. Chapter 6 corresponds to friction factor including related literature reviews and some relevant turbulence models are introduced. Numerical model including governing equations, mesh, geometry and numerical approach are explained in details in chapter 7. Moreover, in chapter 8, based on different turbulence models the validation of CFD results against experimental has done due to choosing the best accurate model for CFD simulations. In chapter 9, whole results including CFD and experimental results regarding wall temperature distribution, heat transfer coefficient and friction factor coefficient are compared and discussed. Chapter 10 mainly focused on validation of different friction factor correlations against CFD results. Finally, chapter 11 devoted to showing velocity and density contours, in follow, chapter 12 is considered as a conclusion.

## 1.2 Brayton cycle vs. Rankine cycle

There are various power cycles for producing heat and electricity, of which steam Rankine cycle and Brayton cycle are the most common types. The usual working fluid in Rankine cycle is water. The cycle converts heat to mechanical work under phase changes in closed loop. Brayton cycle or gas turbine cycle utilizes gas as working fluid without phase changes. In general, Brayton cycles are divided into two types including; Open Brayton cycle, utilizes combustion chamber and closed cycle, uses heat exchanger.

Regarding the efficient power cycle with small initial resource consumption, the most common introduced cycles (Rankin and Brayton cycles) are compared briefly. According to (Ahn, et al., 2015). the different power cycle's conversion with respect to thermal efficiency and inlet turbine temperature is shown through figure 1 .In fact, comparing steam Rankine cycle and Brayton cycle indicated the higher cycle efficiency in steam Rankine cycle due to incompressibility of water, which result in applying less work for pump (considering low inlet temperature for turbine). On the other hand, the utilized air in gas turbine is compressible, which requires more significant compressor work than steam Rankine cycle; consequently, thermal efficiency of Brayton cycle reduces though, turbine inlet temperature is higher (Ahn, et al., 2015).

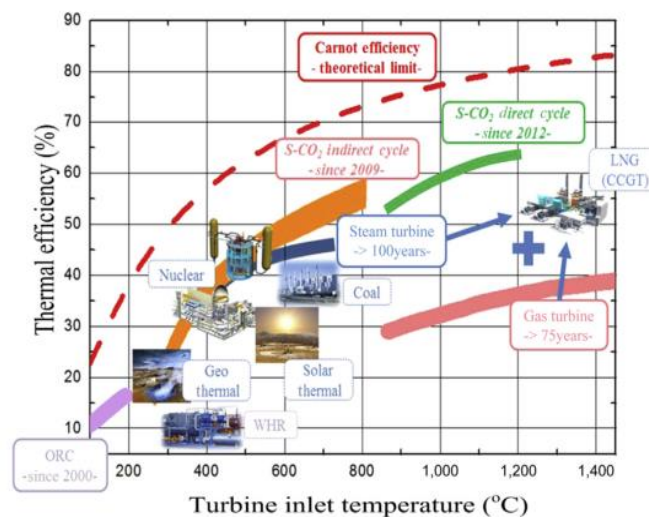


**Figure 1.** Comparing thermal efficiencies of different conversion systems (Ahn, et al., 2015)

Although Brayton cycle has lower thermal efficiency than Rankin cycle, in general, closed Brayton cycle is simple and adjustable for modular based techniques, compact, cost competitive (cheaper than Rankin cycle) and with less construction period, which impacts on interest compared to Rankin cycle. (Dostal, et al.,2004)

To summarise the comparison of Rankin and Brayton cycle, the major reason for high efficiency of Rankin cycle is low pump work and pumping power due to incompressibility of water and regarding Brayton cycle, thanks to high inlet temperature of turbine, which leads to achieve high thermal efficiency in the cycle (Kim, et al.,2016)

### 1.3 Advantages of CO<sub>2</sub> as a working fluid in supercritical phase

There are several investigations about working fluid in supercritical mode, which can affect the cycle efficiency. Although in those studies working fluids (generally based on hydro carbonates and Chloro-fluorocarbons) were operated under 30°C to 40°C critical temperature and some literatures showed increasing cycle efficiency with working fluids like N<sub>2</sub>O<sub>4</sub> (Dostal, et al.,2004) , but they are not interesting for using in Brayton cycle due to their defects such as flammability, environmental damage, corrosiveness and toxicity. Therefore, working fluid for supercritical cycle should be chosen among not very harmful gases. In this regard, some of working fluid examples are presented in table 1 (Feher E.G.,1968)

**Table 1.** Critical conditions for different fluids (Dostal, et al.,2004)

Fluid name	Formula	Critical temperature (°C)	Critical pressure (MPa)
Ammonia	NH <sub>3</sub>	132.89	11.28
Carbon Dioxide	CO <sub>2</sub>	30.98	7.38
Hexafluorobenzene	C <sub>6</sub> F <sub>6</sub>	237.78	2.77
Perfluoropropane	C <sub>3</sub> F <sub>8</sub>	71.89	2.68
Sulfur Dioxide	SO <sub>2</sub>	157.50	7.88
Sulfur Hexafluoride	SF <sub>6</sub>	45.56	3.76
Water	H <sub>2</sub> O	373.89	22.10
Xenon	Xe	16.61	5.88

The CO<sub>2</sub> is a promising working fluid in supercritical Brayton cycles due to moderate critical temperature (not very low and not very high) 30.98 °C and at pressure 7.38 MPa, in which “fractional pressure drops are low, while the cycle still operates at manageable pressure” (Dostal, et al.,2004). SCO<sub>2</sub> Brayton cycle operates above the critical point to maximize the cycle performance as a result of reduction in compressor work. From environmental point of view, CO<sub>2</sub> is non-toxic, nonflammable, with low global warming potential (GWP) approximately 1000 to 3000 times lower than hydrofluorocarbons refrigerants and zero Ozone depletion potential (ODP) (Nikitin, et al.,2006).

#### **1.4 SCO<sub>2</sub> Brayton cycle- Advantages**

As a matter of fact, SCO<sub>2</sub> Brayton cycle is defined as a power conversion, in which the best characteristics of both Rankine and Brayton Cycle are combined in one cycle such as low compressor work close to critical point and moderate turbine inlet temperature respectively (Kim, et al.,2016). The main application of SCO<sub>2</sub> power cycles are in gas turbine turbomachineries, air conditioners, refrigerators, hot water supply, concentrated solar thermal(CST),fossil fuel boilers, geothermal, shipboard propulsion system and nuclear power (Dostal, et al.,2004; Nikitin, et al.,2006). Here the basic SCO<sub>2</sub> Brayton cycle is explained briefly.

The operation of SCO<sub>2</sub> power cycle is similar to ideal Brayton cycle with using CO<sub>2</sub> as a working fluid in system. The operation of cycle is above the CO<sub>2</sub> critical point. It is worth mentioning that, the CO<sub>2</sub> thermophysical characteristics near to the critical point (7.38MPa and 30.98 °C) are highly sensitive with respect to pressure and temperature, which results in changing CO<sub>2</sub> properties in mentioned region. In fact, the main method for developing cycle efficiency is reducing the compressor work near the critical point. The main reason of compressor reduction work is due to CO<sub>2</sub> low compressibility close to the critical point. For example, using CO<sub>2</sub> as a working fluid leads to lower compressor work approximately 30% to 40% than helium. The SCO<sub>2</sub> Cycle operates in lower inlet turbine temperature (550°C) compared to helium Brayton cycle (850 °C) for achieving the same thermal efficiency( 43%), considering pressure at 20Mpa and 8MPa for CO<sub>2</sub> and Helium respectively (Dostal, et al.,2004). Dostal, et al. (2004) claims that the mentioned operation condition and 43% thermal

efficiency achievement of direct cycle, leads to 18% total cost reduction of power plant. Moreover, turbine inlet temperature in  $\text{SCO}_2$  Brayton cycle can be increased due to lower  $\text{CO}_2$  corrosiveness compared to steam at the same temperature (The moderate operation range of temperature for turbine inlet is between  $500^\circ\text{C}$  to  $900^\circ\text{C}$ ) (Was, et al.,2007; Lee, et al.,2014).

In addition, many studies regarding different  $\text{SCO}_2$  cycles carried out by Dostal, et al.(2004) such as inter cooling, reheating, recompressing and pre compressing. Among mentioned cycles, recompression cycle operates in at most  $650^\circ\text{C}$  temperature and at least 20MPa pressure found out with highest efficiency among others (Dostal, et al.,2004). The main reason to justify the recompression cycle high efficiency is higher specific heat in recuperator cold side flow than hot side (about 2 to 3 times), which allows 2 to 3 times more heat transfer in cold side recuperator. In fact, recompressing cycle layout consists of one main compressor and one recompressing compressor as shown in figure 2 .In compare to simple Brayton cycle, recompressing cycle has two recuperators. Flow divided into two parts before pre cooler to make up for  $C_p$  difference in recuperator with low temperature as well as increasing heat transfer in recompressing cycle, which leads to reduce heat rejection effectively and improving thermal efficiency (Dostal, et al.,2004; Ahn, et al., 2015). The lower pressure heat exchanger faces more thermophysical fluctuations than the higher pressure heat exchanger due to vicinity of critical point, shown in figure 3.

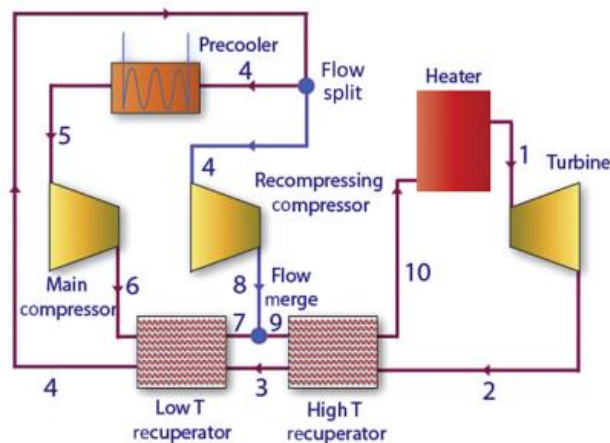


**Figure 2.** Recompression Brayton cycle (RBC) (Ahn, et al., 2015)

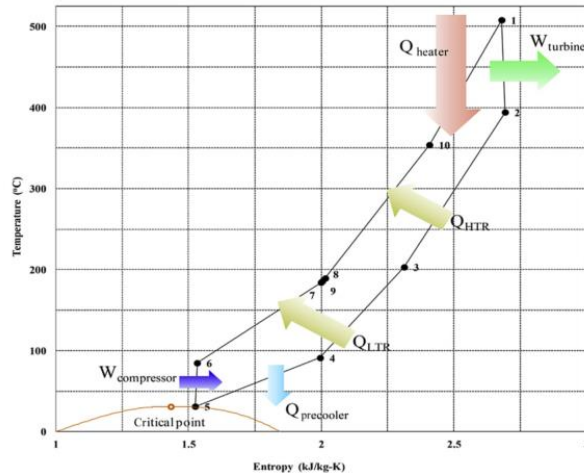


**Figure 3.** Temperature-entropy diagram of RBC (Ahn, et al., 2015)

Following the advantages of  $\text{SCO}_2$  cycle, the small size of turbomachinery is the other essential characteristics. In fact, considering the operation of system in supercritical region, the minimum operating condensing pressure of system specifically by moving away from critical point is higher than both steam Rankine cycle and simple gas Brayton cycle, which representing the reduction of volumetric flow rate due to higher density of  $\text{CO}_2$  near critical point, leads to have significant smaller turbomachinery size approximately 10 times compared to steam Rankin cycle. (Ahn, et al., 2015)

## 2 HEAT TRANSFER AT $\text{CO}_2$ PHASE

Considering the basic rules of heat transfer theory, the temperature difference is a crucial force in order to drive heat transfer. Likewise, based on second law of thermodynamics, heat always transfers from higher temperature to colder temperature of a system. Therefore, the system always is in equilibrium through dealing heat lost by hot medium and heat gained by cold medium. In fact, the amount of transferred heat per unit time is called heat transfer rate. According to “Newton’s Law of Cooling”, convection heat transfer rate is defined by equation 1.(Cenjel,2008):

$$\dot{Q}_{Conv} = hA_S(T_S - T_\infty) \quad (1)$$

Where,  $\dot{Q}$  (Watt) is convection heat transfer rate,  $h$  ( $\text{W}/\text{m}^2 \text{ }^\circ\text{C}$ ) is convection heat transfer coefficient,  $A_s$  ( $\text{m}^2$ ) is Heat transfer surface area,  $T_s$  ( $^\circ\text{C}$ ) is Surface temperature and  $T_\infty$  ( $^\circ\text{C}$ ) is fluid temperature.

For measuring the heat transfer performance in any process the Nusselt number (dimensionless) can be used, which is expressed by equation 2:

$$N_u = \frac{hD}{K} \quad (2)$$

Where,  $K$  ( $\text{W}/\text{mK}$ ) is thermal conductivity,  $D$  (m) is hydraulic diameter.

## 2.1 Thermophysical properties at $\text{SCO}_2$ phase

The focus of following part is on presenting the thermophysical characteristics of  $\text{CO}_2$  in supercritical region due to special characteristics of  $\text{SCO}_2$  near the critical point. It is considering that the critical temperature and pressure ( $30.98 \text{ }^\circ\text{C}$  -  $7.38 \text{ MPa}$ ) of  $\text{CO}_2$  is significantly lower than majority of fluids such as  $\text{H}_2\text{O}$  ( $384.7 \text{ }^\circ\text{C}$ -  $25\text{MP}$ ). The low operating pressure and temperature of  $\text{CO}_2$  was the motivation for investigations by Thiwaan Rao, et al. (2016) used mentioned working fluid. The variation of specific heat, density, viscosity and thermal conductivity with limited temperature range at four supercritical pressure values are depicted in figures 6. Meanwhile, mentioned thermophysical properties can be achieved from NIST- REFPROP using Span Wagner EOS model (Thiwaan Rao, et al., 2016; Lemmon, et al.,2015).

As it is shown in density diagram, by increasing the temperature, density is affected close to the critical point of  $\text{CO}_2$  significantly. Comparing the reduction trends at four different pressure values, observed that the most reduction happened near the critical point. The trends for viscosity and thermal conductivity are the same as density. On the other hand, as it is observed in specific heat diagram, that  $C_p$  near the critical point has reverse trend. It reaches to the highest value close to the critical point. It appears that, as temperature increases, the specific heat reduces at higher pressures. (Thiwaan Rao, et al., 2016)

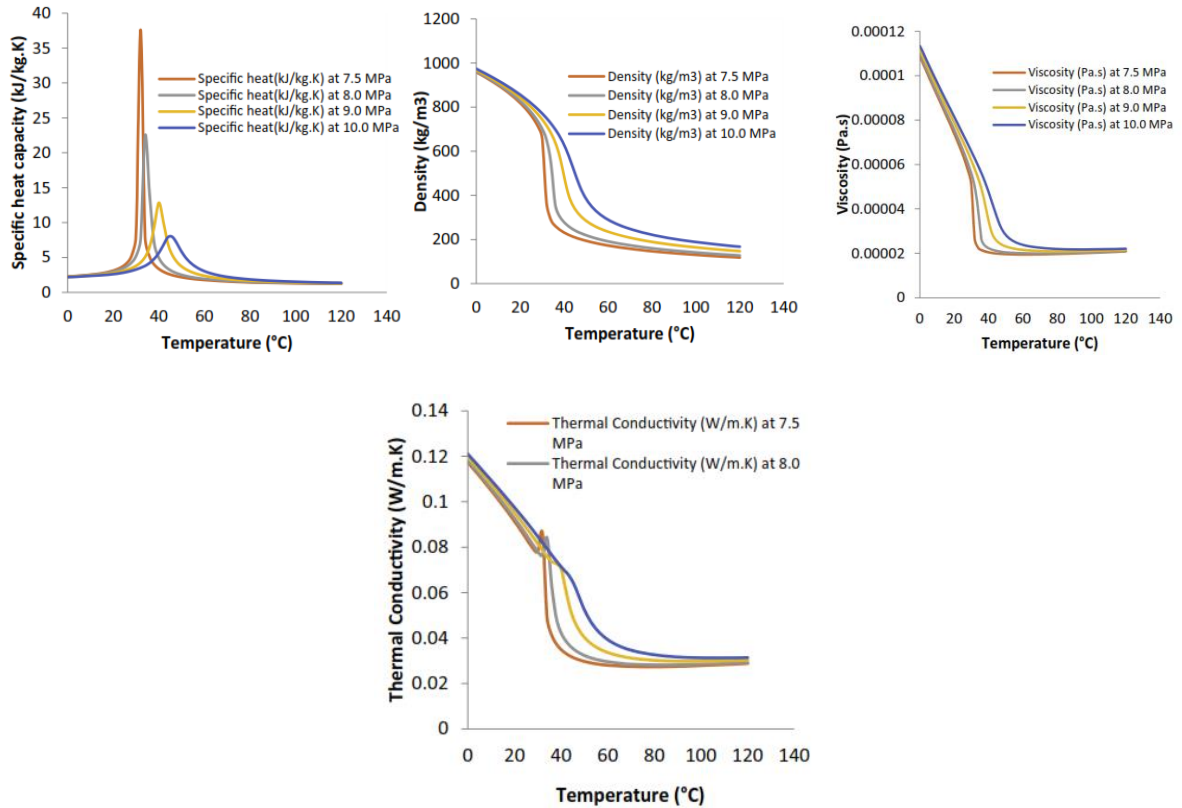


**Figure 4.** Thermophysical properties of SCO<sub>2</sub> near critical point with respect to temperature at different pressures ( Thiwaan Rao, et al., 2016)

### 3 COMPARING REAL GAS AND IDEAL GAS THERMODYNAMIC

This part reviews the substantial concept of thermodynamics that is essential to define the energy transfer process. It includes the real gas equations and their deviations from ideal gas. Studying thermodynamic behavior of real and ideal gas helps to identify the different phenomena related to ideal gas and their effects on heat transfer. In fact, this part starts with basic definition of real gas and ideal gas.

Ideal gas is an imaginary concept for better understanding of real gas behavior, which is more complicated than ideal gas. In ideal gas there is proportional bulky distance between molecules. Therefore, molecular interaction can be neglected. Majority of gases, in extremely low pressure and high temperature behave similar to ideal gases. Gas behavior is determined through volume, pressure, temperature and number of moles. The equation, which connects  $P$ -

$V$ - $T$ , is called equation of state (EOS). The simplest EOS is the ideal gas equation, which is expressed by  $PV = nRT$ , where,  $P$  is pressure,  $V$  is volume,  $n$  is number of moles,  $R$  is gas constant and  $T$  is temperature. On the other hand, in real gas the molecular interaction and volume are considered intensely. In fact, real gas does not obey the ideal gas law and deviation from ideal gas in high pressure and low temperature is observed significantly.

As mentioned above, the pressure, temperature and specific volume of substances are related through equation of states (EOS), which consist of simple to complex equations. The simplest EOS is the ideal gas equation, which predicts the behavior of gas (pressure-volume-temperature) with limited applicability range but more accurate EOS models for the wider range capability is required. In this regard, there are many EOS equations for real gas and the most well-known ones are presented as following parts.

### 3.1 Van der waals

The Van der Waals equation is one of the earliest real gas EOS, proposed in 1873. In fact, this EOS supposed to improve the ideal gas equation by adding intermolecular interaction ( $a/v^2$ ) and molecular occupied volume ( $b$ ).

$$\left(P + \frac{a}{v^2}\right)(v - b) = RT \quad (3)$$

### 3.2 Cubic equation of states

For predicting the real gas behavior properties the cubic EOS are the most convenient types. They are very useful equations in engineering perspective because of limited requirement and simple application based on few parameters including; critical point or acentric factor to predict both liquid or vapor volumes based on known pressure and temperature. Considering the cubic volume, the lowest and highest roots are related to liquid volume and vapor volume respectively. Moreover, they operate with low computational requirement.

### 3.2.1 Redlich Kwong model

Redlich Kwong (RK) model is quite suitable for gas phase and poor for liquid properties. RK model consists of four versions including; Standard Redlich Kwong, Aungier Kwong, Soave Redlich, and finally Peng Robinson. The RK model supposed in 1949, which is “one of the most accurate two parameters corresponding EOS” (ANSYS,2009). The Aungier model is accurate version of RK, especially near the critical point.

The RK model is expressed in equation 4, which is shown in cubic variants.

$$P = \left(\frac{RT}{v-b} - a\right)/T^{\frac{1}{2}} v(v+b) \quad (4)$$

Where,  $v$  is specific volume,  $a$  and  $b$  are constants that represent attractive potential of molecules and volume respectively.

$$a = (0.4275R^2 T_c^{\frac{6}{3}})/P_c$$

$$b = (0.08664RT_c)/P_c$$

### 3.2.2 Standard Redlich Kwong model

This SRK equations is the modified type of RK model, in which

$$a = a_0 \left(\frac{T}{T_c}\right)^{-n}$$

$$a_0 = \frac{0.42747R^2 T_c^2}{P_c}$$

$$b = \frac{0.08664RT_c}{P_c}$$

$n = 0.5$  (Redlitch & Kwong, 1948).

### 3.2.3 Peng Robinson model

As explained before, Peng Robinson model is the version of RK model. In this model, the critical properties as well as acentric factor ( $\omega$ ) are considered, formed more precise equation for substance, specifically near the critical point. The Peng Robinson model is preferred to apply for gas-condensate systems due to better performance in the vicinity of the critical point.

The actual equation of Peng Robinson model is expressed in equation 5 (Redlitch & Kwong, 1948).

$$P = \frac{RT}{(V_m - b)} - \frac{a\alpha}{(V_m^2 + 2bV_m - b^2)} \quad (5)$$

Where,

$$a = \frac{0.457235R^2T_c^2}{P_c}$$

$$b = \frac{0.077796RT_c}{P_c}$$

$$\alpha = (1 + k(1 - T_R^{0.5}))^2$$

$$k = 0.37464 + 1.54226\omega - 0.26992\omega^2$$

$$\omega = -1 - \log_{10}[\rho^{VAP} (T_R)/P_c]$$

$T_c$ ,  $P_c$ ,  $T_R$  and  $\rho^{VAP}$  are critical temperature, critical pressure, reduced temperature and density of vaporization respectively. The concept of reduced temperature and density refers to the ratio of temperature and density to critical temperature and critical density respectively.

### 3.2.4 Span Wagner Model

Cubic EOSs are not accurate model adjacent to the critical point of CO<sub>2</sub>. The most suitable model for predicting the behavior of thermodynamic properties would be Span Wagner model, which is well fit for CO<sub>2</sub>. Initially, Span Wagner equation is modeled with respect to Helmholtz energy and covers thermodynamic properties of CO<sub>2</sub> from the triple point up to 1100K and 800MPa for temperature and pressure respectively (Span & Wagner, 1996).

Span Wagner equation based on dimensionless Helmholtz energy is expressed by equation 6, which is shown dependency on density and temperature.

$$\varphi = A(\rho, T)/(RT) \quad (6)$$

The above equation divided in two parts including: the Ideal gas, shown with superscript  $\varphi^\circ$  and the other part in terms of residual behavior of fluid, shown by  $\varphi^r$ . Both parts are expressed in equation 7.

$$\varphi(\delta, \tau) = \varphi^0(\delta, \tau) + \varphi^r(\delta, \tau) \quad (7)$$

Where  $\delta = \rho/\rho_c$  (inverse reduced density) and  $\tau = T_c/T$  (inverse reduce temperature)

In fact, due to dependency of Helmholtz energy model to density and temperature, the whole thermodynamic properties of fluid is achievable through merging derivatives of equation 7.

First part of Span Wagner EOS is treated almost analytically. In contrast to ideal gas models, the residual models are not treated analytically and they determined empirically based on experimental measurements. The complete EOS equations for both ideal gas and residual part presented by Span Wagner can be find in Span & Wagner (1996).

### 3.3 Compressibility factor

In general, the criteria to determine the deviation of ideal gas from real gas is called compressibility factor, which is shown with  $Z$  in equation 8, where  $V_{ideal} = \frac{RT}{P}$ . This factor defines the deviation from the ideal gas. Compressibility factor for Ideal gas is equal to one and as much as the value of  $Z$  farther away from one, there is more deviation from ideal gas. In fact, real gases, near saturation line as well as critical point deviate from ideal gas significantly.

$$Z = \frac{PV}{RT} \quad , \quad Z = \frac{V_{actual}}{V_{ideal}} \quad (8)$$

In practice, the compressibility factor is determined based on gas compressibility figure with respect to reduced pressure and reduced temperature. The reduced variables are expressed by equation 9 and 10.

$$P_R = \frac{P}{P_{cr}} \quad (9)$$

$$T_R = \frac{T}{T_{cr}} \quad (10)$$

Where,  $P_{cr}$  and  $T_{cr}$  are critical pressure and temperature. Figure 5 shows the compressibility factor of different fluids with respect to reduced pressure and reduced temperature. As it is shown from the figure 5, the highest deviation from the ideal gas is related to fluids with reduced pressure and reduced temperature equal to unity, where it is critical point. Moreover,

as the  $P_R$  gets close to the zero with respect to all temperature ranges, the compressibility factor gets close to unity. In another word, the gas with very small  $P_R$  values without considering the temperature can be assumed as ideal gas. In addition, other interesting observation from figure 5 is that, at the same  $P_R$  and  $T_R$  the compressibility factor is the same for all fluids, which refers to the principle of corresponding state. (Cenjel,2008)

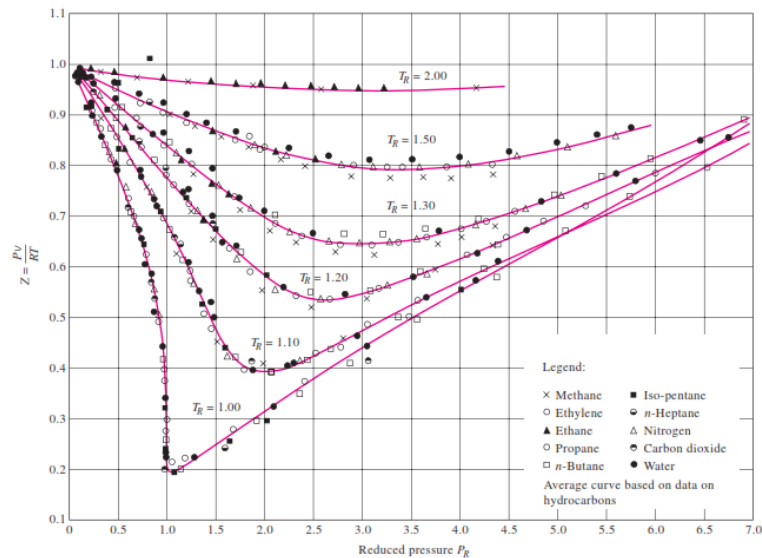


**Figure 5.** Comparing compressibility factors for different gases (Cenjel,2008)

According to (Ahn, et al., 2015) , the compressibility factor of CO<sub>2</sub> reduces between 0.2 to 0.5 near critical point, results in reducing the compression work substantially.

## 4 TYPES OF HEAT EXCHANGERS

According to wide range configuration of heat exchangers, they are commonly classified based on heat transfer process including: direct or indirect contact type, number of fluids including: two fluids/ three fluids or N-fluids, surface compactness including: gas-liquid or liquid-liquid, construction including: tubular, plate type, extended surface and regenerative, heat transfer mechanisms and flow arrangements including: single pass or multi pass (Incropera, et al.,2011). Here, three main types of heat exchangers among different mentioned classification are discussed including: fin type, shell and tube, and compact heat exchangers.

## 4.1 Fin type heat exchanger

This type of heat exchanger is also called extended surface. They commonly used, where fluid has low heat transfer coefficient condition. In fact, extended surface in fin type heat exchanger helps to increase the capacity of heat transfer, which results to increase heat transfer coefficient. Fin refers to the welded piece of metal to outside tube surface or between plates, which increases the area of heat transfer as shown in figure 6. Fin type heat exchanger also use, when high quantity of gases is available both in cooling or heating process. The main disadvantages of fin type heat exchanger are including: high pressure drop, fouling problem near the corner of fins and cleaning problem and finally problems for using slurry fluids (Incropera, et al.,2011).

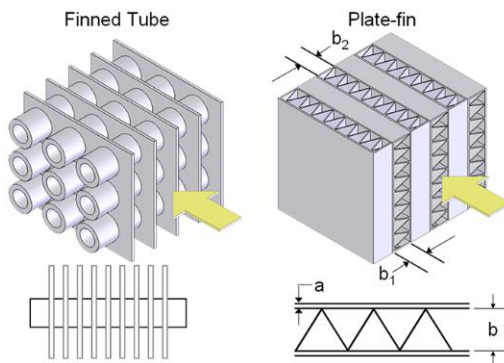


**Figure 6.** Fin type heat exchanger configurations (Incropera, et al.,2011)

## 4.2 Shell and tube heat exchanger:

The basic structure of shell and tube heat exchanger contains tubes, situated inside shell. Basically, the construction involves tubes, passes and baffles as shown in figure 7. Baffles are installed in order to improve convection coefficient of fluid (shell part) with impelling turbulence and velocity. Moreover, baffles are applied to support tubes from vibration. Shell and tube heat exchanger can tolerate temperature up to 900 °C. This type of heat exchanger is widely used in industry due to handle high temperature and pressure, also easy operation and control are the advantages of this heat exchanger. However, the large space requirement and high maintenance cost are considered as disadvantages of shell and tube heat exchanger. (Incropera, et al.,2011)

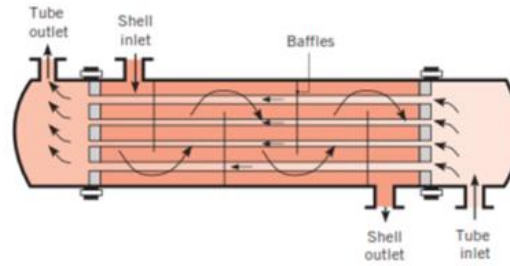


**Figure 7.** Shell and tube heat exchanger configuration (Incropera, et al.,2011)

### 4.3 Compact heat exchanger

This type of heat exchanger typically has dense arrays of fins and tubes or plates. Compact heat exchanger has unique characteristics among other described types. The common working fluid in this type is gas such as gas to gas or gas to liquid for heat exchanger. In fact, heat transfer coefficient of gas is low compared to liquid or solid and fluid flows slowly. Therefore, having large surface is required to achieve a reasonable heat transfer rate. In fact, with less relative volume, more heat transfer surface is available in compact heat exchanger (Incropera, et al.,2011); meaning, heat is transferred in high gas volume and minimum footprint. If the ratio of heat transfer area to volume is larger than  $700 \text{ m}^2/\text{m}^3$  (at least for one side) the heat exchanger (gas to fluid) is characterized as compact (Shah&Sekulic,2003). The advantage of high compactness helps to have higher relative effectiveness with the given pressure drop (Lindstrom, 2005). In fact, achieving high compactness is possible through reduce of passages or adding fins inside passages (Shah&Sekulic,2003).

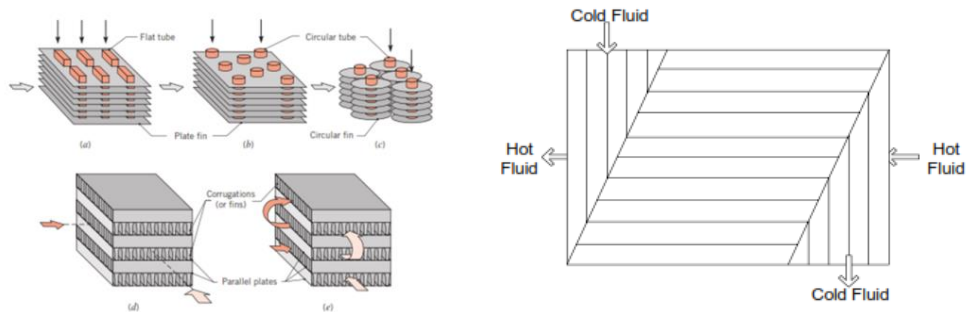


**Figure 8.** Compact heat exchanger configuration (Incropera, et al.,2011)

For improving efficiency of power cycle choosing the right efficient heat exchanger is inevitable. In fact, the two main factors for choosing heat exchanger are considering

compactness and small pressure drop. Therefore, in first stage of selection, the shell and tube heat exchanger would be eliminated due to the large tube diameter, which makes problem for manufacturing and the thick wall tubes due to bearing high pressure differential in heat exchanger (Dostal, et al.,2004). Moreover, according to SCO<sub>2</sub> operation state, thermal efficiency is affected significantly by huge amount of heat recovery in recuperator. Therefore, high effective recuperator is required. Otherwise, increasing capital cost by using shell and tube heat exchanger would be problematic.

In simple CO<sub>2</sub> Brayton cycle, heat exchanger can be considered the largest component based on (Hesselgreaves, et al.,2016). Therefore, size improvement is required; meaning, rather small size of a heat exchanger is an advantage in cooling and heating systems. Regarding compactness of heat exchanger the following information are considered as follow:

Heat exchanger compactness is shown by equation 11, called Colburn  $j$  factor (Nikitin, et al.,2006).

$$j = \frac{D_h}{4L} Pr^{2/3} N \quad (11)$$

Where,  $L$  is length of heat exchanger,  $D_h$  is heat exchanger diameter and  $N$  called number of thermal units, expressed by  $\frac{T_{out}-T_{in}}{\Delta T_m}$ , where,  $\Delta T_m$  defined as mean temperature difference. Based on given condition, both  $Pr^{2/3}N$  and  $j$  are consider as constant values (Hesselgreaves, et al.,2016).

One of the appropriate types of compact heat exchanger for SCO<sub>2</sub> system is called printed circuit heat exchanger with relative high thermal performance as well as small size. In next part, PCHE would be explained in detail due to its prominent features and advantages.

#### **4.3.1 Printed circuit heat exchanger (PCHE)**

The PCHE is a type of compact heat exchanger with prominent features such as high effectiveness, wide operating range, improved safety and cost competitive. The PCHE manufacturing technology is based on photo-etching and diffusion bonding. The structure of PCHE is built on plates made of metal consisting chemical based milled passages of flow. The example of this technology can be observed in electronic manufacturing for printed circuit

boards (Nikitin, et al.,2006) . Next step is joining plates with high temperature and pressure to form blocks, called diffusion bonding process, which causes uniformity throughout sheets leads to heat transfer effectively due to removing resistance between sheets (Song,2007). In addition to high thermal efficiency as a crucial advantage of PCHE, applying photo-etching technology to manufacture heat exchanger causes to keep the size of hydraulic diameter very small, which affects the length of heat exchanger through “keeping same Colburn j factor” leads to reduce the overall power plant cycle size (Saeed & Kim,2017). Besides, “diffusion bonding technology” keeps the core of heat exchanger strength to prevent entering flux, braze and filler, leads to reduce corrosion and improve temperature resistance (Ngo, et al. 2006). PCHE is usually much smaller (about 85%) than conventional heat exchanger type such as shell and tube heat exchanger (Song,2007).

The Printed circuit heat exchangers can tolerate wide range of pressure (approximately 50 MPa) and temperature (approximately 900 °C) due to chemically etched based channels through diffusion bonding process, which makes a uniform mold. The high tolerance of PCHE would be the essential advantage compared to shell and tube heat exchangers. PCHEs are commonly made from stainless steel or duplex steel, alloy based on austenitic, ferritic steel and advanced alloy. The channel diameter should be small enough regarding both efficiency and economic matters. For example for PCHE produced by HEATRIC Company, 2 mm channel diameters is the optimum thermal performance economically (Dostal, et al.,2004). In fact, increasing the channel diameter impacts the size of etched metal, leads to raise the heat exchanger total cost. It can be summarized from above description, that increasing the channel diameter would not be the appropriate choice to have larger flow area but for removing this problem employing double channels or reducing length or angle of waves are recommended. In fact, configuration of channels and etched plates can be optimized for improving heat transfer efficiency; meaning, the optimization process includes the combination of thermal hydraulic as well as economical design, which considers small size, cost and thermal efficiency. Figure 9 shows the components of PCHE while manufacturing. Meanwhile, manufacturing process is explained in detail by Hesselgreaves, et al.(2016).

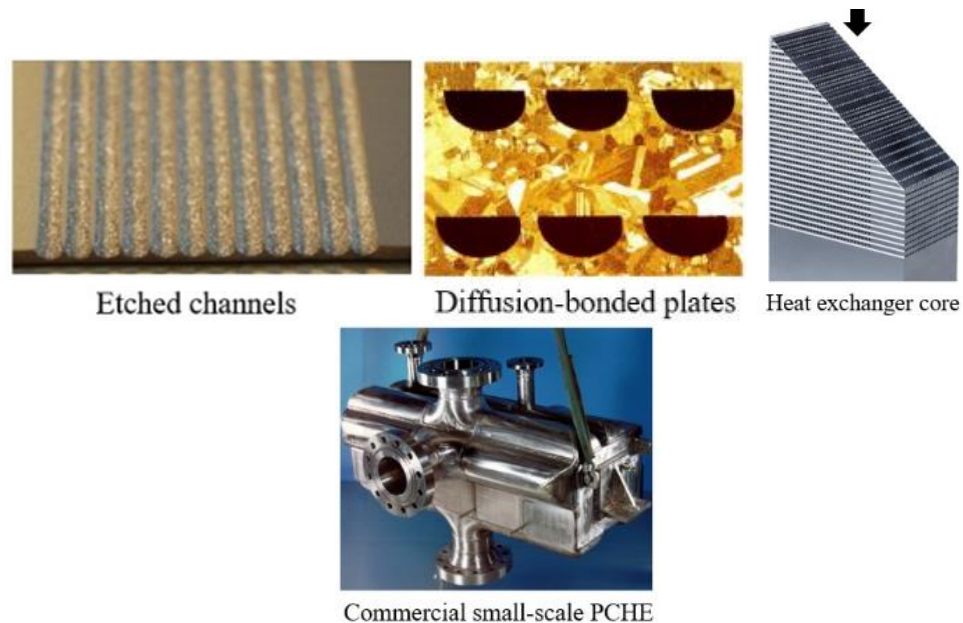


**Figure 9.** PCHE components during manufacturing (Zhang,2016)

Presenting the different types of geometrical surfaces is necessary for better understanding the described designs of following literature reviews. Figure 10 shows the four PCHE channel types including: straight, zigzag, S-formed and airfoil fin from left to right side.



**Figure 10.** Different PCHE channels: straight, zigzag, S shaped and air foil (from left to right) (Zhang,2016)

The straight and zigzag channels are common types of channel found in Heatric Company. Due to structural etched channel in parallel way, cross mixing of flow cannot occur in any type of channels in figure 10. The zigzag or sinusoidal channel can be formed based on etching technique in curved sharp bend shape. The S-formed channel was proposed by Tsuzuki, et al.(2009) at TIT (Tokyo institute of technology) institute with aim of reducing pressure drop with considering to maintain thermal performance. Also, the airfoil channel was introduced by Kim, et al.(2008) because of similar motivation to reduce pressure drop through modifying geometry surface design.

Although PCHE is a new product to the market, it is used in wide range of industrial applications. That is why, in recent years many researches have been carried out about  $\text{SCO}_2$  printed circuit heat exchanger. Regarding heat transfer coefficient and effectiveness based on Kim, et al.(2016) investigation, “thermal and hydraulic performance of 3 KW  $\text{SCO}_2$ - PCHE was studied experimentally. The effectiveness of mentioned heat exchanger was 99% and they found logical dependency between pressure loss and heat transfer coefficient with  $2400 < Re < 6000$  (hot side) and  $5000 < Re < 13000$  (cold side). Also direct relation observed between increasing pressure of  $\text{CO}_2$  and average heat transfer coefficient. D. Eok Kim et al.(2008) did the same three dimensional numerical study using CFD code. They employed extensive range of Reynolds numbers. They studied zigzag channel fin based PCHE. Besides, airfoil channel with low pressure loss was introduced. They compared their CFD results with Ishizuka, et al.(2005) experimental data. Validation of temperature and pressure results showed, well fit agreement between numerical results and experimental data. In further numerical investigation (Kim, et al.,2014), Nusselt number and Colburn j factor of PCHE was checked. To improve heat transfer, they proposed different thickness PCHEs as well as reversed plate structure.

Ngo, et al.(2007) numerically examined the S formed micro channel and zigzag fin PCHE. They introduced pressure drop and Nusselt number correlations with  $3500 < Re < 22000$ .

## **5 PARAMETERS AFFECT FLOW AND HEAT TRANSFER IN $\text{SCO}_2$ HEAT EXCHANGER**

In this part main features that affect the behavior of heat transfer in  $\text{SCO}_2$  heat exchanger described and some previous related researches are mentioned briefly in heating or cooling process.

### **5.1 Tube diameter**

In general, without considering the mass and heat flux, as the tube diameter is smaller in both cooling and heating process, the performance of heat transfer would be better; meaning, heat transfer coefficient inversely is correlated to tube diameter based on  $Nu_D = hD/K$  (considering the constant value of  $Nu_D$ : 3.66 for laminar flow). (Incropera, et al.,2011)

According to (Oh & Son,2010; Kim, et al.,2004; Dang&Hihara, 2004), heat transfer coefficient of horizontal macro tubes in cooling system with  $\text{SCO}_2$  was studied. All tests were done in pseudocritical area. They observed the enhanced effect of smaller inner diameter tube on increasing heat transfer coefficient effectively at different temperatures. Liao&Zhao, (2002) investigated the  $\text{SCO}_2$  heat transfer in six mini tubes with inside diameters from 0.5 mm to 2.16 mm. Results showed the direct relation between decreasing the inner tube diameter and Nusselt number.

## 5.2 Channel characteristics

Tube channel with higher mass flux has smaller temperature changes along the channel compared to lower mass flux in the same channel; meaning, tube with higher mass flux has higher temperature compared to tube with lower mass flux. However, the tube with lower mass flux may have larger channel surface area, which leads to improve heat transfer as well as lowering temperature throughout the channel.

Although most investigations have done to find out the features of  $\text{SCO}_2$  heat transfer in straight tubes, some researches have used serpentine and helical tube including: Xu,R. et al.(2015) applied serpentine tube, Xu,J. et al.(2015) and Zhang, et al.(2015) applied helical formed tube. According to investigation by Thiwaan Rao, et al.(2016) temperature distribution along the tube in serpentine formed (tube diameter: 2.1mm, heat flux: 22.4  $\text{KW/m}^2$ , mass flow rate: 0.00028 kg/s), helical formed (tube diameter: 9mm, heat flux: 20.5  $\text{KW/m}^2$ , mass flow rate: 0.0131 kg/s) and straight tube channel (tube diameter: 9.8 mm, heat flux: 20  $\text{KW/m}^2$ ) were compared respectively. Results showed the higher temperature distribution in serpentine compared to helical tube with considering lower mass flow rate in serpentine tube. Regarding helical tube due to larger surface area than two others, the increase of wall temperature was higher compared to other tubes (Thiwaan Rao, et al., 2016).

## 5.3 Surface heat flux

In this part rather complicated effect of heat flux on heat transfer would be explained profoundly. According to  $q'' = h(T_s - T_m)$ , heat transfer coefficient has correlation directly with heat flux; consequently, heat transfer coefficient is inversely correlated to  $(T_s - T_m)$ ,

where  $T_s$  is wall temperature and  $T_m$  is mean temperature along the tube. On the other hand, heat flux has correlation with  $C_p$  based on equation 12.

$$q_{conv} = \dot{m} C_p (\Delta T) \quad (12)$$

In supercritical region, near the critical temperature and pressure, specific heat reaches to peak value because by increasing heat flux in tube, the temperature of wall and mean fluid temperature increase, leads to dominating the mean fluid temperature over critical temperature. It is worth mentioning that, the difference between wall temperature and mean fluid temperature may fluctuate based on other items such as pressure or mass flux.

In general, when wall temperature is higher than mean fluid temperature, increasing heat flux can affect both thermal conductivity and  $C_p$  at vicinity of wall, which return to increasing heat transfer. When wall temperature is smaller than mean fluid temperature, with considering the similar trend of increasing heat flux, the  $C_p$  may reduce; meaning, increase of heat flux does not lead to increase of heat transfer.

The effect of heat flux on heat transfer coefficient is rather controversial because some cons and pros are found in different literatures. For example, Kim, et al.(2008) showed the inverse correlation of heat transfer coefficient with heat flux for supercritical water. However, in another literatures, (Kim & Kim,2010;Kim & Kim,2011) investigated the correlation between heat flux and temperature along the tube in SCO<sub>2</sub> system and the result showed as heat flux increased, temperature increased inside tube as well as bulk temperature. Li, et al.(2010) compared heat transfer performance of 2mm vertical tube diameter with CO<sub>2</sub> working fluid in upward and downward flow states. Result showed, as heat flux decreased in upward flow tube, the Nusselt number increased, but in downward flow tube, by increasing heat flux, the Nusselt number of CO<sub>2</sub> increased.

## 5.4 Inlet pressure

As explained in part 2.1 the thermophysical features of CO<sub>2</sub> change very sharp near critical point. Generally, pressure drop and inlet pressure are inversely proportional. Increasing inlet pressure leads to increase viscosity and density. Considering, temperature condition higher

than critical temperature, pressure drop decrease due to increasing inlet pressure (Thiwaan Rao, et al., 2016).

According to investigation of Dang & Hihara (2004) which was based on 3 different ranges of inlet pressure including: 8 to 10 MPa for CO<sub>2</sub> in cooling process, results showed at pseudocritical temperature, the heat transfer coefficient was maximum ; meaning , as Pressure increases from 8 to 10 MPa, heat transfer coefficient decreases from 17 to 10 kW/m<sup>2</sup>k. The similar results were achieved by Son & Park(2006).

## 5.5 Inlet temperature

Investigating tube inlet temperature indicates different phenomenon in early stage and alongside a tube. In overall, for both CO<sub>2</sub> cooling and heating process, as inlet temperature increases, the heat transfer coefficient increases following at early stage of tube but when the flow progresses throughout the tube, the phenomena for cooling and heating process is different. In cooling process, when inlet temperature increases, heat transfer coefficient keeps rather constant because the temperature difference between surface temperature and flow temperature ( $T_s - T_f$ ) reduces and specific heat ( $C_p$ ) would reduce either based on equation 13.

$$h = \frac{\dot{m}C_p(\Delta T)}{(T_s - T_f)} \quad (13)$$

In heating process, increasing inlet temperature causes to reduce heat transfer coefficient. In this case ( $T_s - T_f$ ) increases while  $C_p$  decrees; consequently, based on the equation 13, heat transfer coefficient reduces clearly.

Referring to experimental and numerical study of Jiang, et al.(2009) about SCO<sub>2</sub> in cooling process to evaluate heat transfer coefficient, heat transfer coefficient for first stage (first half part) of tube with 70 °C inlet temperature was lower than inlet temperature with 55°C , in despite of that it was observed the almost same heat transfer coefficient after half of the tube region. The maximum heat transfer coefficient is in first quarter of inlet tube region.

## 5.6 Inlet mass flux

In general, although high mass flux helps to increase heat transfer performance, considering only high mass flux can lead to reduce the heat transfer performance, where heat flux is low or temperature is not close to critical temperature. Moreover, with assuming high mass flux, when  $C_p$  is low and viscosity is high, the heat transfer performance can be deteriorated. In  $\text{SCO}_2$  system, high heat transfer performance requires high heat flux, hence, the mass flux should be increased sufficiently based on  $q'' = \dot{m} C_p (\Delta T)$ . Otherwise, with low mass flux,  $C_p$  should be high; therefore, temperature of  $\text{CO}_2$  should be kept near critical temperature. Bruch, et al.(2009) investigated the effect of mass flux in downward vertical tube with  $\text{CO}_2$  working fluid. In supercritical region the direct relation was observed between increasing mass flux and heat transfer coefficient, but in lower temperature range the results showed the inverse dependency of heat transfer coefficient with mass flux.

## 5.7 Pressure drop

Generally, the reason of pressure drop in supercritical system corresponds to frictional resistance (friction factor coefficient), blocked local flow, flow acceleration and gravity. To estimate pressure drop in  $\text{SCO}_2$ , the common equation is expressed by correlation 14 between friction factor ( $f$ ), density of fluid ( $\rho$ ), velocity ( $v$ ) and  $L/D$  = length of tube/diameter of tube

$$\Delta P = f \cdot \frac{L}{D} \cdot \frac{\rho v^2}{2} \quad (14)$$

Equation 15 is extracted from equation 14 as following:

$$\Delta P = f \cdot \frac{L}{D} \cdot \frac{G^2}{2\rho} \quad (15)$$

Where,  $G$  ( $\text{kg/m}^2\text{s}$ ): Mass flux per area

From above equations, it can be described that  $\Delta P$  has reverse correlation with inlet pressure because as inlet pressure in a system increases, following density increases (considering  $G$  is constant) and flow velocity decreases based on equation 16.

$$G = \rho v \quad (16)$$

Considering the system with fluid flow, the flow velocity has direct correlation with friction factor, which is the effect of pressure drop as it is shown by equation 14.

It is realized from above part that near the critical point, density decreases significantly as it was shown in part 2.1. Therefore, flow velocity increases, which leads to increase friction and pressure drop in the system specifically near the critical point.

Moreover, similar to above mentioned concepts as mass flux increases (considering density is constant), flow velocity increases together with increasing pressure drop.

It can be concluded that pressure loss is affected by three main factors including: inlet pressure heat flux and friction factor.

## 6 FRICTION FACTOR

In general, determining friction factor coefficient inside pipe, in case of supercritical operating condition, plays a crucial role regarding design, flow simulation and analysis of pressure drop inside heat exchanger. Friction factor inside pipe have been investigated based on three flow regimes including: laminar, transitional and fully turbulent regime (Nikuradse,1950). Friction factor in laminar regime is expressed by equation 17 called Fanning friction factor:

$$f = \frac{1}{4} \frac{D_h}{L} \left( \frac{\Delta P}{0.5 \rho v^2} \right) \quad (17)$$

Where,  $D$  is pipe diameter,  $L$  is length of pipe,  $\Delta P$  is pressure drop,  $\rho$  is fluid flow density and  $v$  is fluid velocity inside pipe. For scaling the turbulent region the formula,  $f = \frac{64}{Re}$  is employed which is the combination of friction factor and Reynolds number. Friction factor for turbulent regime is expressed by equation 18 called Darcy friction factor.

$$f = \frac{D_h}{L} \left( \frac{\Delta P}{0.5 \rho v^2} \right) \quad (18)$$

The development of Darcy friction factor results to introduce many correlations such as Blasius, Filonenko, Morrison and etc. In next part, some literatures about friction factor in supercritical regions would be reviewed.

## 6.1 Past studies

In Chu & Laurien (2016) the heat transfer in  $\text{SCO}_2$  PCHE was studied. The investigation was based on Direct Numerical Simulation (DNS) for small tube diameter 1 and 2 mm and low Reynolds number for inlet ( $Re = 5400$ ). Due to buoyant effect inhomogeneous friction factor coefficient trend was observed close to the wall.  $C_f$  distribution on bottom wall was higher than top wall in all cases. The calculated inlet friction factor was match with Blasius correlation with just 15% deviation. Besides, velocity distribution was enhanced through flow stratification.

According to Saeed & Kim (2017), to achieve performance evaluation criteria (PEC) (formula defined in detail in Saeed & Kim (2017)), due to gaining thermal and hydraulic performance, Nusselt number and friction factor in zigzag channel PCHE was calculated. The numerical results with wide range of Reynolds number ( $2500 < Re < 30000$ ) validated against 7 friction factor correlations in other literatures, including: Ishizuka, et al.(2005), Ngo, et al.(2006), Nikitin, et al.(2006), Kim, et al.(2008), Ishizuka extended (Saeed, et al. 2017), Ngo extended (Saeed & Kim,2017), and Nikitin extended (Saeed & Kim,2017). Besides, in cold side channel Ngo, et al. and Kim, et al. showed the best agreement with CFD results and in hot side channel, Kim et al. had the best adjustment with CFD results. Moreover, comparison of friction factor and Reynolds number in not same fin structure showed, higher friction factor in cold side than hot side (considering the higher Reynolds number in cold side). Besides, increasing fin angle (between  $20^\circ$  to  $30^\circ$ ) caused to decrease friction factor in PCHE and led to decrease PEC in both hot and cold channels( between 2% to 4%).

Based on Saeed&Kim (2017), the experimental friction factor correlation with  $2500 < Re < 30000$  is introduced as following bellow:

$$f = -2 \times 10^{-6}Re + 0.0467 \quad (19)$$

Ngo, et al.(2006) suggested numerical friction factor correlation with  $3500 < Re < 22000$  as following:

$$f = (0.3390 \pm 0.0285)Re^{-0.158 \pm 0.009} \quad \text{for hot side} \quad (20)$$

$$f = (0.037 \pm 0.1293)Re^{-0.154 \pm 0.036} \quad \text{for cold side} \quad (21)$$

Moreover in literature Ngo, et al.(2006), the new S channel PCHE working with CO<sub>2</sub> proposed and its capability compared to CO<sub>2</sub>-H<sub>2</sub>O (gas-liquid) PCHE. The results showed lower volume (3.3 times) of new S-shaped PCHE compared to gas –liquid PCHE. Besides, the pressure drop in gas-gas PCHE was 37% lower than gas liquid system.

To predict the local heat transfer coefficient as well as pressure drop in SCO<sub>2</sub> PCHE the developed empirical friction factor correlation with Reynolds number range between 2800 to 12100 by Nikitin, et al.(2006) was proposed as following:

$$f = (-1.545 \pm 0.099)10^{-6}Re + (0.09318 \pm 0.00090) \quad \text{for hot and cold side} \quad (22)$$

The heat transfer coefficient was not constant and it changed between 300 to 650 W/m<sup>2</sup>K. The compactness was 1050 m<sup>-1</sup>. The results showed that the PCHE with mentioned characteristic is suitable choice for CO<sub>2</sub> cycle.

According to Kim, et al.(2008) the numerical friction factor correlation applied for wide range of Reynolds number between 2000 to 55000.

$$f = (0.2881 \pm 0.212)Re^{-0.1322 \pm 0.0079} \quad (23)$$

In this literature pressure drop and heat transfer characteristics between CO<sub>2</sub> PCHE with zigzag channel and suggested new airfoil fin channel compared. Numerical results showed no specific changes about heat transfer rate per volume between models but the pressure drop in airfoil fin shape calculated 1/20 of zigzag channel.

Several friction factor correlations in SCO<sub>2</sub> system surveyed by Pioro, et al.(2004). The Numerical analysis for hydraulic resistance in SCO<sub>2</sub> system showed that there is no accurate turbulent model for prediction of fluid characteristics, specifically with high heat fluxes due to sharp changes of properties between critical point and pseudocritical region.

## 6.2 Boundary layers and universal law of wall

Boundary layer is a thin layer of fluid near the surface and this layer has velocity gradient and thermal gradient as it is shown in figure 11. Velocity gradient causes due to friction between

fluid and solid surface. Flow velocity varies from zero ( $u = 0$ ) close to solid surface to  $u_\infty$  in free stream of fluid; meaning, where  $Y^+ = 0$ , velocity gradient is maximum and where  $Y^+ = \delta$ , ( $\delta$  is thickness of boundary layer) velocity gradient is zero. The velocity difference between layers provides shear stress in fluid flow. Besides, heat transfer from solid surface to fluid causes thermal gradient, in which temperature changes from surface ( $T_s$ ) to free stream ( $T_\infty$ ).

From heat transfer point of view, thermal boundary layer causes low temperature changes between solid surface and first thin layer of fluid (sub layer). Therefore, heat transfers quite slowly ( $dT/dy \sim 0$ ) but in turbulent region the temperature changes between solid surface and closest layer increases due to having big eddies; consequently, heat transfer increases.

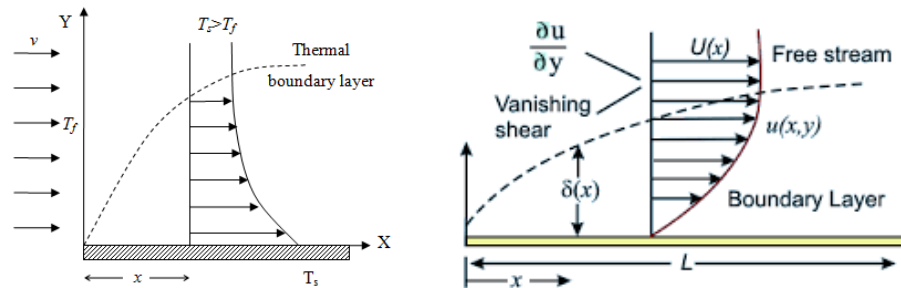


**Figure 11.** Thermal and velocity gradient (from left to right) (Module 4,2018;Laminar boundary layers,2018)

The “distribution of velocity based on boundary layers” shown in figure 12, can be separated into three parts, including: viscous sub layer which is the nearest layer to surface, log layer or buffer layer and defect layer or fully turbulent layer, which is the outer layer. In viscous sub layer (inner layer) flow is laminar and molecular diffusion causes the momentum and heat transfer in fluid because due to no surface slip condition the generated eddies are small with short life time. In outer layer or defect layer, turbulent and eddies are the reason of momentum and heat transfer because of large eddies with relative long life time.

In fact, eddies play crucial role to heat transfer from lower relative warm layers closed to surface to cold upper layers. Moreover, eddies transfer kinetic and momentum energy from higher velocity layers (up layers) to lower velocity layers (down layers close to surface); consequently, turbulent flow causes higher heat transfer rather than laminar flow.

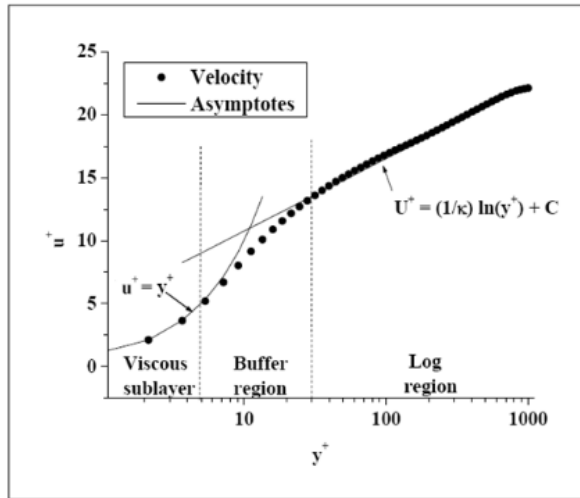


**Figure 12.** Velocity distribution in boundary layers (Fatima,2010)

Resolution of viscous sub layer for modeling at the vicinity of wall should be highly considered.

Famous dimensionless equations for modeling close to the wall surface are introduced as following: Dimensionless velocity:

$$u^+ = \frac{u}{u_r} \quad (24)$$

Where,  $u_r = \sqrt{\frac{\tau_w}{\rho}}$  which is named friction velocity consisting  $\tau_w$ , wall shear stress and  $\rho$ , flow density.

Dimensionless distance ( $y^+$ ) shown by equations 25.

$$y^+ = \frac{\rho u_r y}{\mu} \quad (25)$$

Due to dependency of viscous sub layer to  $u_r$ ,  $\nu = \frac{\mu}{\rho}$  and  $y$  the dimensionless equation 26 is introduced.

$$u^+ = f(y^+) \quad (26)$$

As explained before in viscous sub layer there is no surface slip condition; therefore, at  $y = 0$  Reynolds shear stress  $-\rho\overline{u'v'} = 0$  and Reynolds number ( $Re = \frac{\rho U y}{\mu}$ ) approaches to zero; meaning, flow is laminar and velocity is correlated with  $y$  (near the surface) linearly; therefore, the velocity profile in mentioned region expressed by  $u^+ = y^+$ .

In log layer, velocity profile correlates to  $y$  logarithmically.

In fully turbulent layer, the velocity profile can express by equation 27, this region is called law of logarithmic.

$$u^+ = \frac{1}{\kappa} \ln(y^+) + C \quad (27)$$

Where,  $\kappa$  is von Karman constant and  $C = 5.45$ . (Wilcox,1998)

### 6.3 Turbulence models

In general, Reynolds Average Navier Stokes (RANS) based turbulence equations are classified into eddy viscosity and Reynolds stress models, including some sub models. In this part, those examined sub models for this study are introduced briefly, however each type consists more sub models than those explained here.

- Eddy viscosity models: including Standard K- $\epsilon$  model and Standard K- $\omega$  model
  - K- $\epsilon$  model turbulence model would be accurate and this model is widely used to predict flow in engineering applications with respect to robustness and accuracy. (ANSYS Inc.,2014)
  - K- $\omega$  SST model:  $\omega$ -equations are developed to predict internal and external flow separation, which is very essential application in aerodynamic field. The k- $\omega$  SST turbulence model is applied for highly accurate prediction of separating flow based on adverse pressure gradients (ANSYS Inc.,2006). This model has the characteristics of both K-  $\omega$  model in the vicinity of wall and K- $\epsilon$  model in free stream. This model covers wide range of flows including low turbulence Reynolds number and high turbulence Reynolds number (with low turbulence in viscous sub layer) accurately (ANSYS Inc.,2006).The generic form of K-  $\omega$  SST turbulence equation is as following:

$$\frac{\partial(\rho\mu_j)}{\partial x_j} = \frac{\partial}{\partial x_j} \left[ \Gamma_k \frac{\partial k}{\partial x_j} \right] + G_k - Y_k + S_k \quad (28)$$

$$\frac{\partial(\rho\omega\mu_j)}{\partial x_j} = \frac{\partial}{\partial x_j} \left[ \Gamma_\omega \frac{\partial \omega}{\partial x_j} \right] + G_\omega - Y_\omega + D_\omega + S_\omega$$

Where,  $G_k$  is kinetic energy of turbulence model,  $G_{k\omega}$  is  $\omega$  generation,  $\Gamma_k$  and  $\Gamma_\omega$  are k and  $\omega$  effective diffusivity.  $Y_k$  and  $Y_\omega$  are k and  $\omega$  dissipation.  $D_\omega$ ,  $S_k$ ,  $S_\omega$  are cross diffusion and user defined source terms respectively.

- Reynolds stress models (RSM): including SMC- $\omega$  (Omega Reynolds Stress) and Explicit algebraic Reynolds stress model(EARSM).
  - Omega Reynolds Stress is employed to avoid issues including: the boundary layer simulation in  $\varepsilon$  equations, predict of slow separation in  $\varepsilon$  equations and low Reynolds number integration in  $\varepsilon$  equations.
  - EARSM model allows extending two equation models. The model comes from Reynolds stress transport equation (ANSYS, Chapter 4).

## 7 CURRENT MODEL: COMPUTATIONAL FACT

This thesis investigates the heat transfer characteristics of turbulent  $\text{SCO}_2$  such as mainly friction factor and heat transfer coefficient inside horizontal pipe with 3D steady state turbulence flow models. Due to lack of data regarding printed circuit heat exchanger, the horizontal pipe (about 4 m) was used instead of PCHE .The inside pipe diameter is 22.14 mm under state of unchanged heat flux. In current model the range of employed Reynolds number is  $1 \times 10^5 < Re < 5 \times 10^5$  validated against experimental results to analyze the effects of friction factor coefficient in details.

### 7.1 Governing equations

In this part, the governing equations (Navier -Stokes) for solving the convective heat transfer in  $\text{SCO}_2$  as well as employed turbulence models are discussed. Modeling this problem is based on numerical approach, which built from modeled mathematical objects, comes from differential or integral equations and the solution is obtained through finite volume

discretization technique based on discretize of governing equations into algebraic equations. In this study the CFX tool, which employs finite volume technique is used for simulation. In fact, finite volume technique predicts the mentioned governing equations over volume. CFX solves continuity, momentum and energy equations. The appropriate models when there is turbulence in fluid flow are K- $\epsilon$  and K- $\omega$  SST model in order to solve kinetic energy as well as dissipation equations. In fact, for choosing suitable turbulence model, different factors are required such as accuracy level, accessible computational resource and computational time. Most common and well know turbulence models are two equations turbulence models ( $\omega$  based and  $\epsilon$  based models).The Navier-Stokes equations calculated for steady flow in this report are continuity, momentum and energy equations as following:

$$\frac{\partial(\rho U_j)}{\partial x_j} = 0 \quad (29)$$

$$\frac{\partial(\rho U_i U_j)}{\partial x_j} = -\frac{\partial P}{\partial x_i} + \frac{\partial}{\partial x_j} \left( \mu \left( \frac{\partial U_i}{\partial x_j} + \frac{\partial U_j}{\partial x_i} \right) \right) \pm \rho g \delta_{i1} \quad (30)$$

$$\frac{\partial \rho h}{\partial x_i} (\rho u_i H) = \frac{\partial}{\partial x_i} \left[ \left( k + \frac{C_p \mu_t}{Pr_t} \right) \frac{\partial T}{\partial x_i} \right] \quad (31)$$

Where,  $\mu$  is molecular viscosity,  $\mu_t$  is turbulent viscosity,  $k$  is thermal conductivity,  $Pr$  is prandtl number,  $H$  indicates enthalpy,  $\rho = \rho(P_0, h)$ ,  $\mu = \mu(P_0, h)$ ,  $C_p = C_p(P_0, h)$ .

## 7.2 Geometry, mesh grid and boundary conditions

For validating heat transfer characteristics and turbulence model of  $\text{SCO}_2$ , the employed experimental results are according to Adebisi & Hall(1976) study. The cross section mesh grid of pipe is shown in figure 13. Mesh dependency test has done and shown results in figure 14, indicates that by increasing the structured mesh around 1300000 cells, wall temperature does not change. Near the walls, cell sizes are quite small to achieve  $y^+ < 1$ . The horizontal tube shown in figure 15, with internal diameter 22.14 mm is divided into heating (2.44m) and adiabatic part (1.22m). All experimental conditions are considered for computational modeling of test 1.1, test 1.2, test 2.1 and test 3.1, which are shown in table 2. The applied experiment is near  $\text{CO}_2$  critical point at pressure 7.6 MPa, temperature 30.98 °C and with changeable inlet mass flow rate about 0.035kg/s to 0.15kg/s ( from test 1.1 to 3.1).

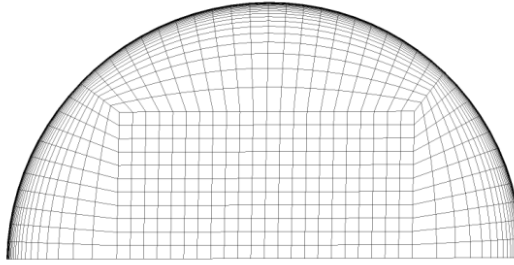


**Figure 13.** Cross section of mesh grid used in simulation

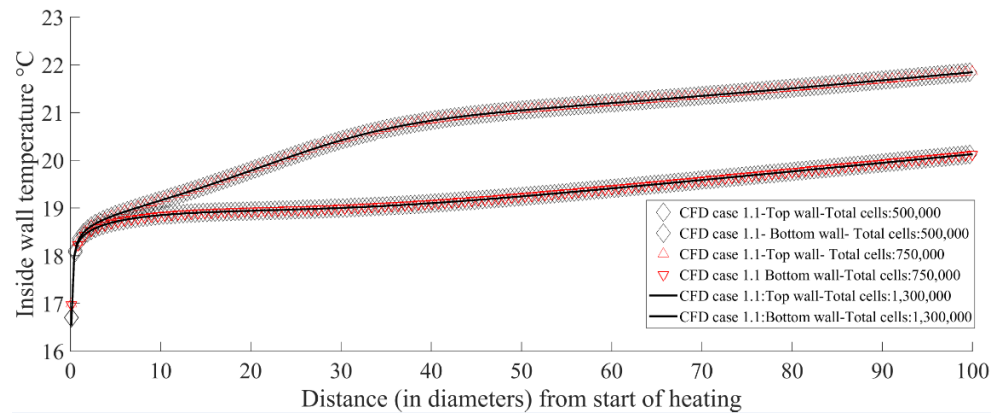


**Figure 14.** Mesh dependency test for CDF case 1.1 with coarse mesh (total cells: 500000) and fine mesh (total cells: 1300000)

The numerical model is 3 dimensional steady state turbulence flow with symmetric flow field inside pipe. Figure 16, shows the operating range of heat exchanger in numerical simulation. Black arrow demonstrates the area of inlet and outlet temperature of four simulated tests at pressure 7.6 MPa. The temperature/pressure points of each test are shown with colorful points. The red colors, blue points and green points show the inlet and outlet operating temperature in test 1.1-1.2, 2.1 and 3.1 at pressure 7.6 MPa respectively. The vicinity of operating range of heat exchanger to critical region can affect high thermophysical fluctuation, results in having high efficient heat exchanger.

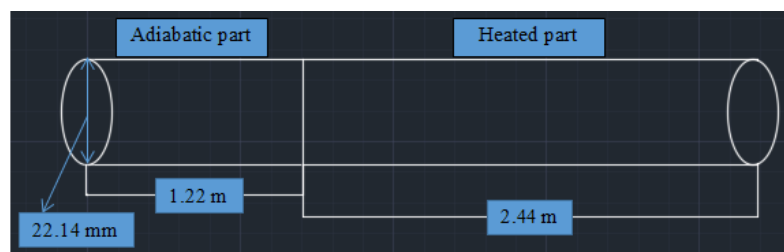


**Figure 15.** Schematic of the numerical model

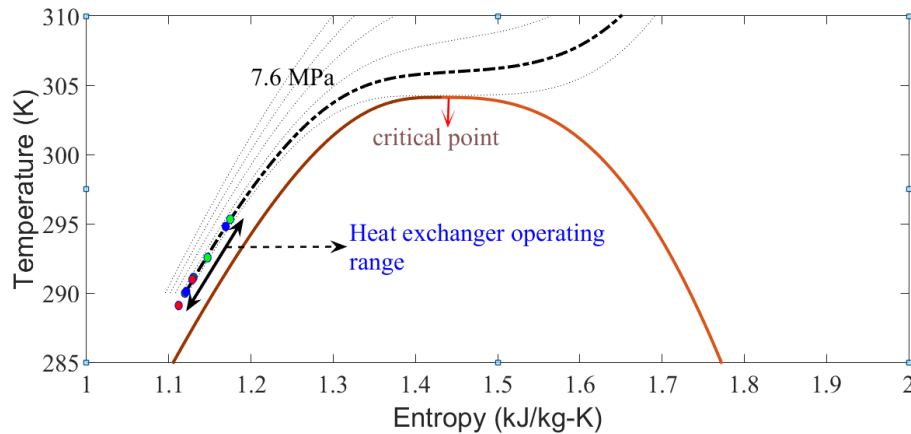


**Figure 16.** Operating range of investigated heat exchanger

**Table 2.** Experimental conditions (Adebiyi & Hall,1976)

Test code	Mass flow rate (kg/s)	Inlet bulk temperature (°C)	Average heat flux (kW/m <sup>2</sup> )	Outlet bulk temperature (°C)	Test pressure (MN/m <sup>2</sup> )
1.1	0.151	15.9	5.3	18.1	7.586
1.2	0.148	15.4	15.1	21.3	7.59
2.1	0.0773	14.2	5.2	18.4	7.603
3.1	0.080	19.7	5.1	23.2	7.607

Creating good mesh is required to realize appropriate thermodynamic details of fluid flow. The structured mesh grid of pipe consists of about one million total cell numbers. Boundary layer specifically mesh grid close to the wall should be determined perfectly in order to have accurate computational values regarding wall shear stress as well as heat transfer coefficient. Numerical results with respect to mesh distribution are more vulnerable for turbulent flow compared to laminar flow because of major interaction between mean flow and turbulence. Therefore, correct mesh resolution is highly required to resolve value of gradients close to the wall. To prevent numerical error and computational time raise, finer mesh near the wall regions and coarser mesh in the middle of tube are considered, shown in figure 13 .The dimensionless distance to the wall expressed by  $y^+$  should be smaller than 1 ( $y^+ < 1$ ); meaning, the first mesh node close to the wall should be placed in viscous sub layer area in order to address the resolve of flow details accurately. It should be mentioned that the above mentioned area includes at least 5 grid, where  $y^+ < 1$ . Set boundary conditions are

including: inlet pressure and temperature, outlet mass flow rate, all walls are defined as no slip and constant heat flux is added to the heating wall. All remain surfaces are considered as symmetric boundary conditions.

### 7.3 Numerical approach

The CFX solver, which is finite volume based CFD solver used for all numerical simulation. Considering turbulence model, SST K- $\omega$  is used in present simulation due to its advantages compared to K- $\epsilon$  close to the wall as well as K- $\omega$  regarding bulk flow. The convincing details of choosing turbulence model will be discussed in part 8 regarding temperature distribution validations. To determine thermophysical properties of CO<sub>2</sub>, specifically temperature and pressure “NIST standard reference database” is employed. In fact, RGP table is used as real gas look up table of properties to define material and coupled with CFX solver. AlFa RGP application creates RGP table from Span Wagner equation in NIST standard reference data base. As explained before, Span Wagner EOS is the best model to predict CO<sub>2</sub> thermophysical properties. The RGP dependency test has been studied in (Ameli, et al. 2016; Ameli, et al.,2018). For RGP dependency test maximum 1000 points chose for temperature and pressure. The resolution of RGP table was increased since; wall temperature did not show any dependency to the table resolution.

To discretize momentum and energy equations, high resolution scheme is used in order to achieve high numerical accuracy. In fact, residual errors of all governing equations are less than  $10^{-5}$ .

For checking convergence, different criteria are observed such as energy, mass and momentum imbalance approached to constant zero value. Also, the observed RMS for mass and momentum is less than  $10^{-5}$  in all tests. Figure 17 shows the convergence results through imbalance (energy, mass and momentum), and RMS (mass and momentum) for each CFD test.

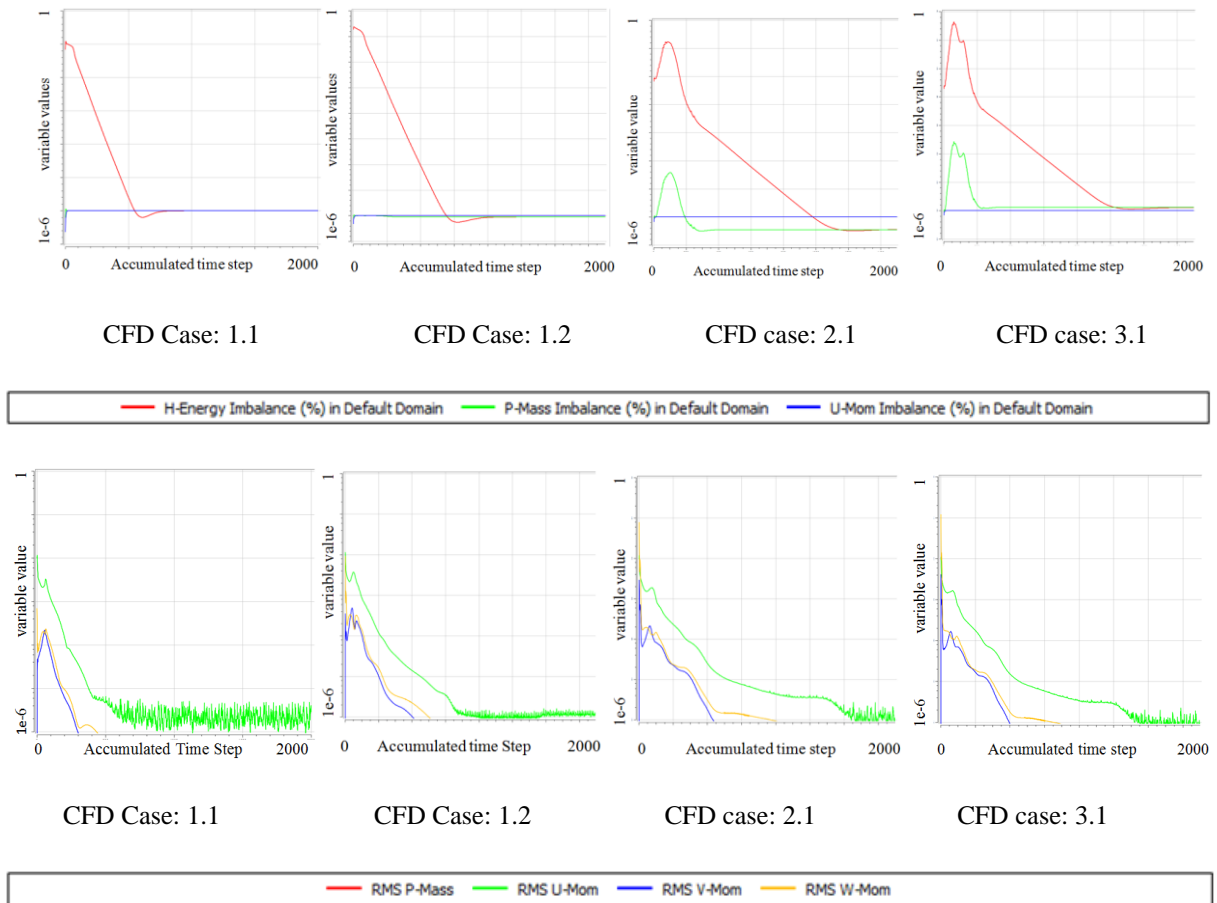


**Figure 17.** Convergence result of CFD cases

## 8 COMPARISON AND VALIDATION OF NUMERICAL MODEL WITH EXPERIMENTAL DATA

The experimental approach that is used for validation of numerical model is Adebisi & Hall (1976) experimental data. According to their experiments, the measured temperature distribution was changeable along the pipe due to effect of buoyancy. Moreover, they placed welded thermocouples at top and bottom wall with different angles due to gain temperature distribution along the pipe Adebisi & Hall (1976). In this part the four different turbulence models examined in numerical simulation compared to experimental results based on test 1.1 conditions in order to find the most accurate turbulence model for continuing numerical computation. Figure 18 presents inside wall temperature distribution of four turbulence models including:  $k-\omega$  SST (shear stress transport),  $k-\epsilon$  EARSM, Omega Reynolds Stress (ORS) and

standard k- $\epsilon$  with respect to the starting point of heated wall ( $x/d = 0$ ). The heat flux in test 1.1 is  $q=5300 \text{ W/m}^2$ , which is constant. The mass flow rate is  $0.151 \text{ kg/s}$  and the inlet temperature and pressure are  $15.9 \text{ }^\circ\text{C}$  and  $7.586 \text{ MPa}$  respectively. In all tested turbulence models, the temperature difference are shown qualitatively. The SST turbulence model works quite accurate narrowly followed by ORS model. Specific temperature values in standard K- $\epsilon$  and K- $\epsilon$  EARSMS models show the huge discrepancy. Consequently, the selected turbulence model for numerical computation is considered k- $\omega$  SST because of its best accordance to experimental results.

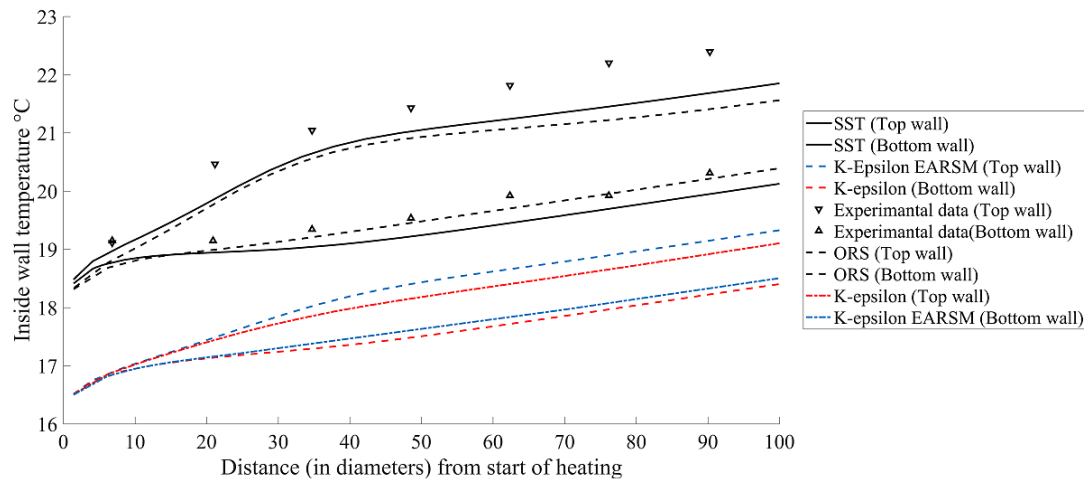


**Figure 18.** Validation of wall temperature distribution simulated by different turbulence model against Adebisi & Hall (1976) experimental results

## 9 RESULTS AND DISCUSSION

### 9.1 Wall temperature distribution

In this part numerical results of CFD cases regarding temperature distribution inside pipe from start of heating section compared with experimental results in test 1.1, 1.2, 2.1 and 3.1 shown in figure 19. It can be seen that in test 1.1 and 1.2 there is appropriate consistency for top and bottom wall temperature between CFD and experimental results but in test 2.1 and 3.1 the trend is followed with a bit difference in top wall temperature. In all four cases, temperature distribution tends to increase in both top and bottom wall uniformly and due to buoyancy effect the top wall has higher temperature than bottom wall. The highest temperature,

specifically on top wall can be seen in test 1.2 due to highest heat flux  $q=15100 \text{ W/m}^2$  compared to other cases. In case 3.1 the sharp change is observed at the start of heating condition, which may correlate to high inlet temperature of pipe or less mass flow rate. In all cases, except case 1.1 with highest mass flow rate, the sharp temperature changes happened at the beginning of top wall heating sections and then temperature continues to increase rather constant. The bottom walls in all cases show rather constant temperature increment without special sharp change.

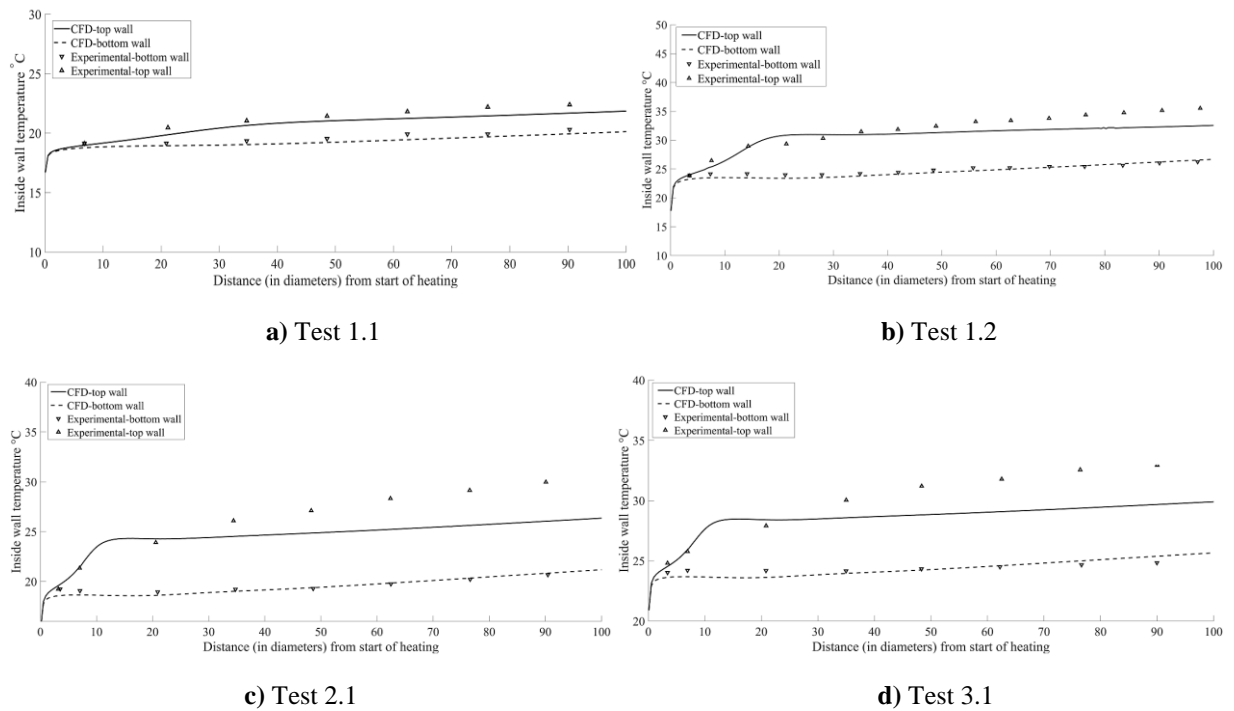


**Figure 19.** Temperature distribution of numerical results based on SST turbulence model against experimental results in four test conditions

## 9.2 Heat transfer coefficient

In this part heat transfer coefficient of  $\text{SCO}_2$  along the heating wall is investigated in four mentioned tests. The heat transfer is computed based on equation 32.

$$h = \frac{q}{(T_w - T_b)} \quad (32)$$

Where,  $q$  is heat flux,  $T_w$  expresses top / bottom wall temperature and  $T_b$  represents bulk temperature. Bulk temperature determines the mass flow average temperature at each cross section surface. It can be seen that in all cases of figure 20, the heat transfer coefficient along the pipe in bottom wall is higher than top wall because the top wall temperature is higher than bottom wall. Therefore, with considering the constant heat flux, the difference between wall temperature and bulk temperature is higher in top wall than bottom wall, leads to decrease heat transfer coefficient in top wall. On account of all tests in figure 20, heat transfer coefficient in top walls for all tests has stronger changes than bottom walls. The highest heat transfer coefficient is found in bottom wall in case 1.2 due to highest heat flux  $q=15,100 \text{ W/m}^2$  than other cases. Observing all tests, the heat transfer coefficient has a rather sharp change, specifically in top walls, from start of heating up to distance 35 diameters along the heating section in test 1.1, 20 diameters in test 1.2, 10 diameters in test 2.1 and 3.1, and then the value of heat transfer coefficient continues rather constant in all cases. As it is observed, the sharpest change is shown in test 1.2, which has the highest heat flux.

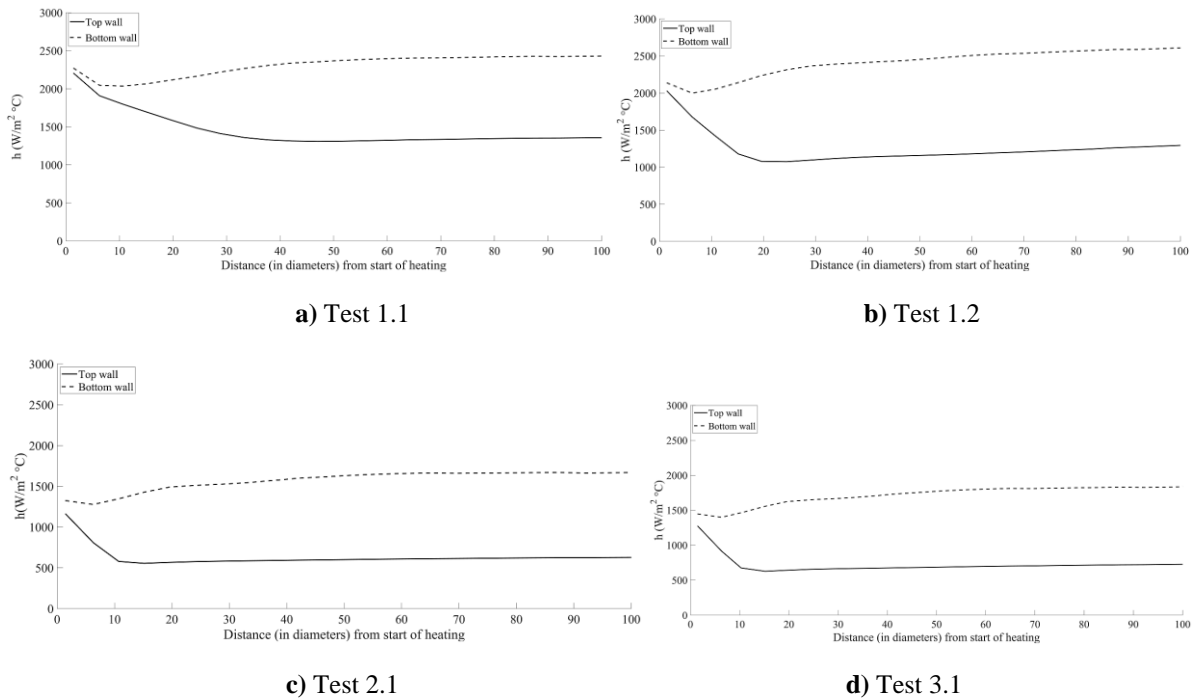


**Figure 20.** Heat transfer distribution of numerical results based on SST turbulence model in four test conditions

### 9.3 Friction factor coefficient

In general, for fluid flow inside pipe, three types of forces are considered including: viscous force, friction force and buoyancy. Considering fluid flow inside horizontal pipe, friction exists at the interface of fluid and wall pipe, which is the main reason of kinetic/enthalpy loss. Friction factor term determines the pressure loss because of wall friction. The generic equation of friction factor is expressed by equation (33).

$$f = \frac{\tau_w}{\frac{1}{2}\rho u^2} \quad (33)$$

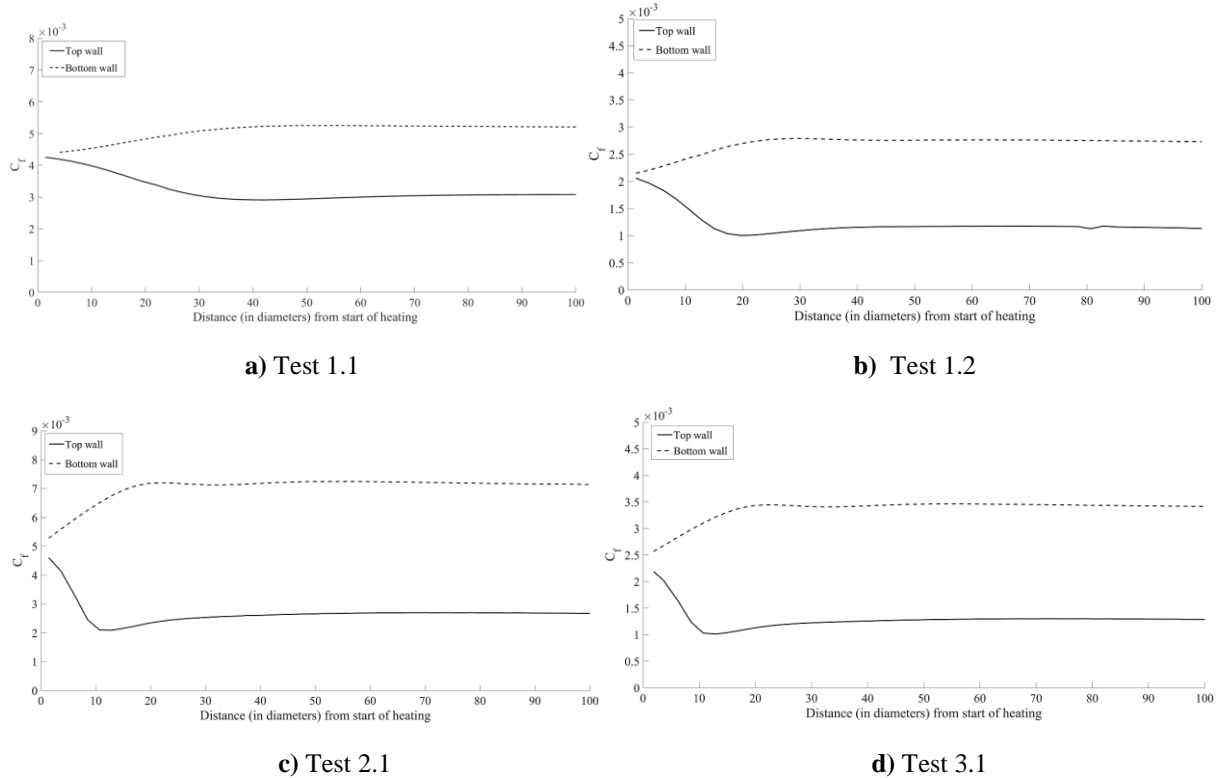
Where,  $\tau_w$  is wall shear stress,  $\rho$  is bulk density and  $u$  is the bulk fluid velocity.

Figure 21 shows the results of average friction factor coefficient in top and bottom wall of each case individually. It is observed that in all cases, friction factor coefficient in bottom wall is higher than top wall due to higher shear stress on bottom surface as a result of applied buoyancy force. In case 1.1, 1.2, 2.1 and 3.1, inlet friction factor coefficients are about 0.0042, 0.0022, 0.005 and 0.0025, respectively.

The sharpest change of friction factor from start of heating can be observed in top and bottom wall in test 2.1 and 3.1 with lower mass flux compared to other cases. The friction factor coefficient at the start of heating of case 1.1 and 1.2 with higher mass flux shows the smoother change than test 2.1 and 3.1.

The friction factor coefficient has rather similar trend like heat transfer coefficient: meaning, it shows strong increase or decrease at start of heating in both top and bottom walls and then after distance 35, 20 and 10 diameters from start of heating in test 1.1, 1.2 and 2.1 or 3.1 the figures continue constant.

The averaged friction factor of the adiabatic part of the pipe has been calculated and compared with average friction factor of heating wall, presented in table 3.



**Figure 21.** Friction factor coefficient of numerical results based on SST turbulence model in four test conditions. It can be noticed that, by increasing the heat flux (from test 1.1 to 1.2), averaged friction factor value faces bigger change from adiabatic to heated part. The same trend has been noticed for mass flow rate (from test 1.2 to 2.1). By increasing heat flux from test 1.1 to 1.2 the effect of buoyancy force becomes stronger because of increasing the temperature difference between top and bottom wall. Therefore, friction factor gets sharp fluctuation at the start of heating part. The same trend has been noticed for mass flow rate. Reducing mass flux in half from case 1.2 to 2.1 affect the noticeable change on average friction factor at adiabatic (11.7%) to heated section (4.5%) of pipe.

**Table 3.** Comparison of average friction factor in heating wall with adiabatic wall for numerical tests

Test code	Average of $C_f$ (Heating wall)	Average of $C_f$ (Adiabatic wall)	Changes (%)
1.1	0.0041	0.0044	5.8
1.2	0.0039	0.0044	11.7
2.1	0.0048	0.0050	4.5
3.1	0.0046	0.0049	5.2

## 10 VALIDATION OF DIFFERENT FRICTION FACTOR CORRELATIONS AGAINST CFD RESULTS

The aim of this part is validating existing friction factor correlations mainly in horizontal pipe with turbulence, against present CFD results. The list of used correlations is shown in table 4.

**Table 4.** List of friction factor correlations used in validation

Data source	Correlation	Range of $Re$	References
Blasius (1913)	$C_f = 0.316 (Re)^{-0.25}$	$Re \leq 10^5$	(Blasius,1913)
Blasius R	$C_f = 0.079 (Re)^{-0.25}$		(Blasius,1913)
Filonenko	$C_f = (1.82 \log(Re) - 1.64)^{-2}$	$10^4 \leq Re \leq 5 \cdot 10^6$	(Monaghan, et al.,1953)
Wilcox(1995)	$C_f: 1/\sqrt{f} = -2 \log(2.51/Re\sqrt{f})$	$Re > 3000$	(Wilcox,1998)
Wilcox	$C_f = 0.045 (Re - 0.25)$		
Lee	$C_f = 0.0018 + 0.152 (Re)^{-0.35}$	$Re > 3000$	((Blasius,1913)
Jensen	$C_f = 0.0412 (Re)^{-0.1925}$	$Re > 3000$	(Jensen, et al.,1999)
Prandtl (1927)	$C_f = 0.074 (Re)^{-0.2}$	$Re > 4000$	(Prandtl,1926)
Prandtl-Schlichting	$C_f = 0.455 \log(Re)^{-2.58}$	$Re > 4000$	(Schlichting,1979)
Kempf-Karman (1951)	$C_f = 0.055 (Re)^{-0.182}$	$Re > 3000$	(Monaghan, et al.,1953)
Granville (1977)	$C_f = 0.0776 (\log(Re) - 1.88)^{-2} + 60 (Re)^{-1}$	$Re > 3000$	(Samson & Sidum,2015)
Genielinski	$C_f = (0.79 \log(Re) - 1.64)^{-2}$	$Re > 3000$	(Gnielinski, 1976)
Prandtl (Denn)	$C_f = 0.255 \log(Re)^{-2.5}$	$3000 \leq Re \leq 5 \cdot 10^6$	(Mori, et al,2009)
Morrison	$C_f = \frac{0.0076 \cdot (3170/Re)^{0.165}}{(1 + (3170/Re)^7) + 16/Re}$	$10^2 \leq Re \leq 10^7$	(Morrison,2013)

The simplest correlation to compute skin friction factor is Blasius correlation (1913), which is obtained from first principle of non-Newtonian fluid flow (Blasius,1913). Filonenko

correlation has gained from Darcy friction factor equation. According to Fang, et al.(2001) both Blasius and Filonenko friction factor equations are suitable for smooth tubes (wall with small roughness elements) with turbulent flow (Monaghan, et al.,1953).Wilcox friction factor equation is extracted from (Wilcox,1998). Parndtle (Denn) is modified version of Prandtle equation extracted from Mori, et al.(2009) and Prandtl-Schlichting equation (Schlichting,1979). Kempf-Karman, Granville can be found in (Monaghan, et al.,1953; Samson&Sidum,2015) respectively. Morrison equation meets all ranges of Reynolds number for smooth pipes (Morrison,2013).

Figure 22 shows the comparison of 12 above mentioned friction factor correlations against CFD results. The experimental data are extracted from Adebisi & Hall (1976). Moreover, Dang & Hihara (2004) experimental data for SCO<sub>2</sub> in 2 mm horizontal tube (Inlet temperature: 30 °C to 70 °C, Mass flux: 800 kg/m<sup>2</sup>s, Heat flux: 12 KW/m<sup>2</sup>, Pressure between 30 to 70 MPa) is added in order to show the effect of tube diameter on friction factor coefficient at the same operational Reynolds number range. Here, the average friction factor of top and bottom wall in each test (Adebisi & Hall (1976)) has been calculated and titled by CFD case 1.1,1.2,2.1 and 3.1 in context. Moreover, the Reynolds numbers are calculated based on  $Re = \frac{\rho v D}{\mu}$  at the inlet of heating for each CFD case. The comparison of 12 friction factor correlations and CFD results with Reynolds number range between  $9 \times 10^4$  to  $12 \times 10^4$ , indicate that CFD case results(average friction factor coefficient) have good agreement with predicted friction factor coefficient by Blasius, Wilcox 1995, Morrison and Lee correlations. In the same boundary condition and the same Reynolds number range, experimental data (Dang-Hihara) with smaller tube diameter (2 mm), is quite close to compared correlation including: Blasius R and Genielinski.

It is obvious that CFD case 1.1 is quite close to predicted friction factor coefficient by Wilcox 1995, Blasius, Morison and Lee correlations. CFD case 1.2 has the best match with Wilcox 1995 correlation. CFD case 2.1 and 3.1 are both close to Blasius, Lee and Morrison friction factor correlations. The Dang – Hihara experimental data has good agreement with both Blasius R and Genielinski friction factor correlations. To put in another way, the figure 22 shows that in general, the good friction factor correlation for particular fluid flow is depended

on different factors such as, Reynolds number and tube diameter. Therefore, it is very hard to determine which friction factor correlation is the best for CFD cases.

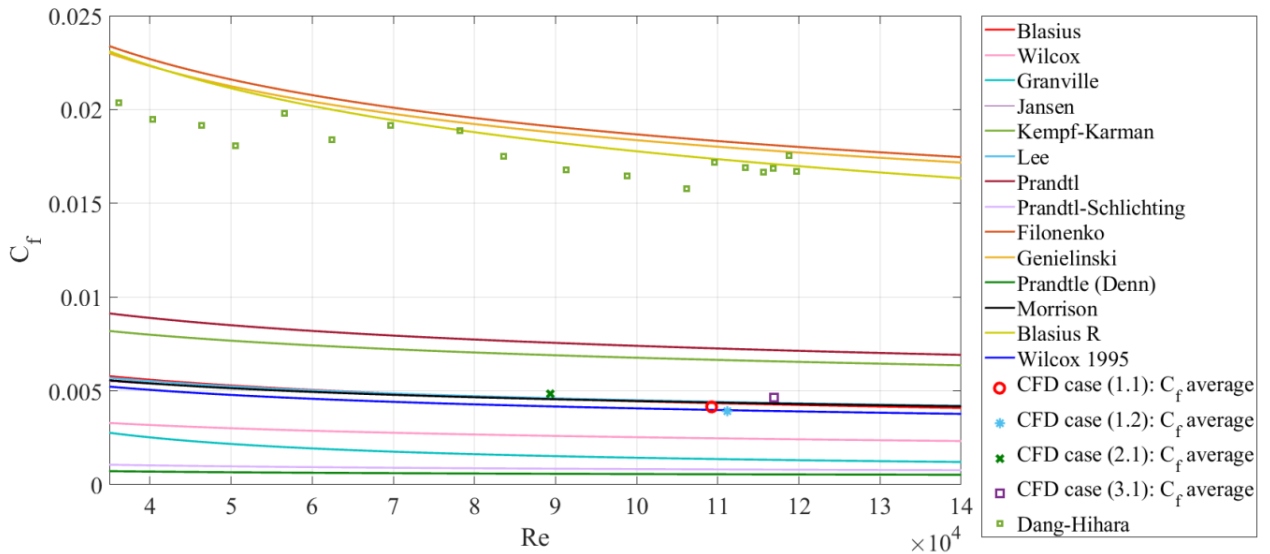


**Figure 22.** Validation of numerical results of friction factor coefficient (averaged -top/bottom wall) against some friction factor correlations

Figure 23, shows the analogy of friction factor coefficient in top and bottom walls of CFD cases with compared friction factor correlations. Considering the higher temperature on top wall than bottom wall of tube, the friction factor coefficient of top walls in CFD cases 1.2, 2.1 and 3.1 have good agreement with predicted friction factor coefficient by Wilcox correlation. The top wall of CFD case 1.1 shows some deviation from other cases, stays between Wilcox and Wilcox 1995. On the other hand, CFD results of bottom walls, which are influenced by buoyance force, have the best agreement with predicted friction factor coefficient, used Kempf-Karman correlation, particularly seen in CFD case 2.1 and 3.1. The CFD results of bottom wall for test 1.1 and 1.2 with some degree of deviation are rather close to predicted friction factor coefficient, used Blasius, Morrison and Lee correlations.

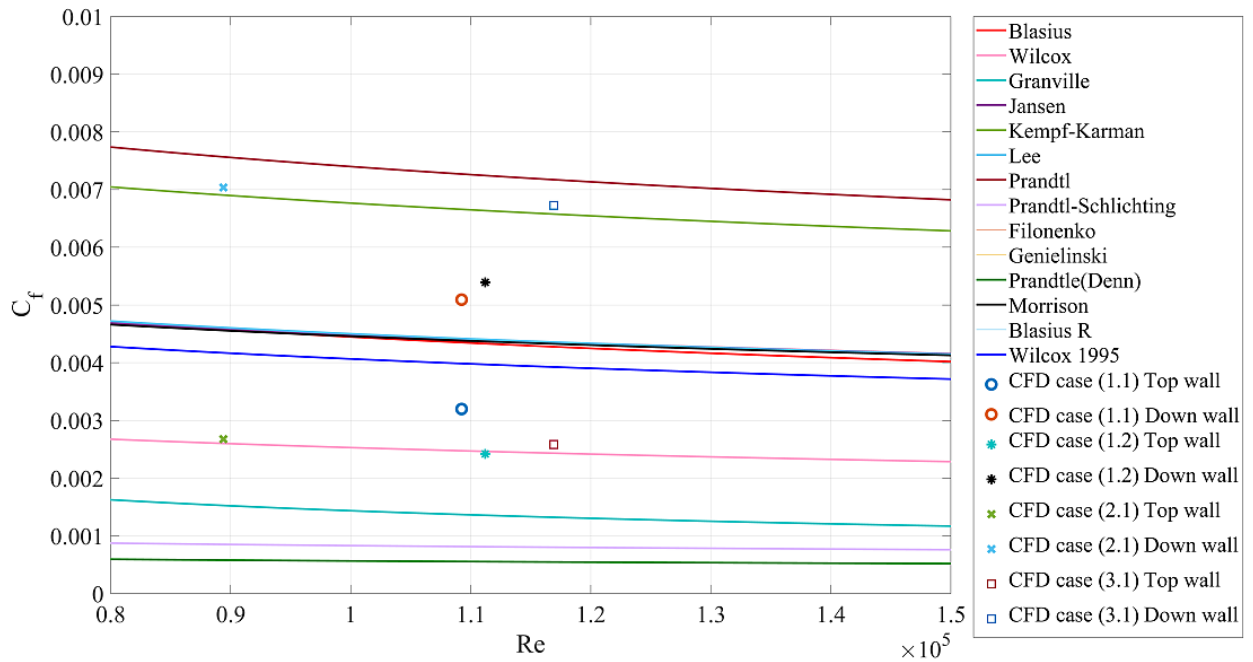


**Figure 23.** Validation of numerical results of friction factor coefficient (top/bottom wall) against best match friction factor correlations

## 11 VELOCITY AND DENSITY CONTOURS

In this part, density and velocity contours along the heating part for test cases are being discussed. Figure 26 presents the contours of normalized velocity and density for numerical test 1.2 with highest heat flux compares to other cases, on cross section surfaces along the heating part of the pipe. The selected cross sections presented in figure 25 for showing velocity and density are named by the number of section's order along the heating pipe, times diameter of pipe including, 4D,14D,30D and outlet section. Velocity contours are observed axisymmetric on planes 4D, (close to start of heating part). First,  $\text{SCO}_2$  is heated near the wall; consequently, density reduction occurs. Considering the constant inlet temperature at test case 1.2, by applying a constant heat flux, sharp temperature gradient appears close to the wall leads to large density changes throughout the pipe, which causes strong buoyancy force. Flow with lower density goes up ward due to the buoyant force and higher density fluid is placed downward. Following density contours, it is observed in all cases that flow in inlet sections are

more uniform than downstream sections. According to figure 24, upward flow is adjacent to the wall, while the downward flow goes in the middle of pipe.

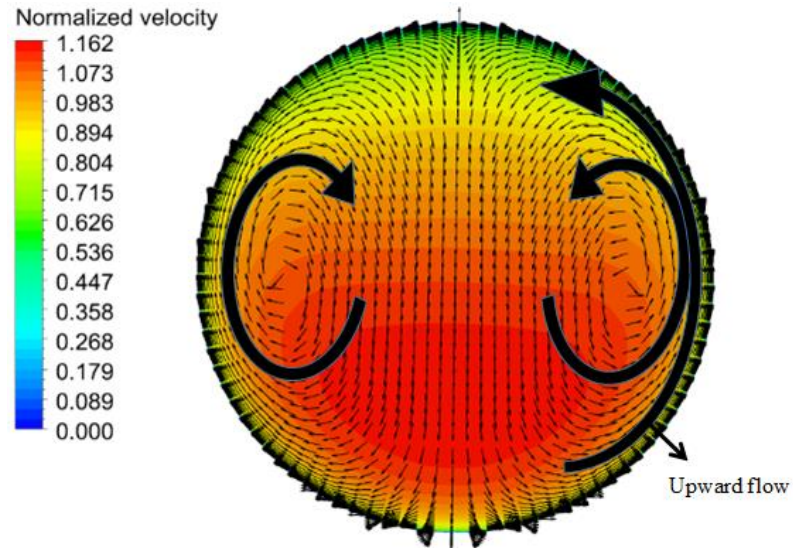


**Figure 24.** Velocity contour cross section

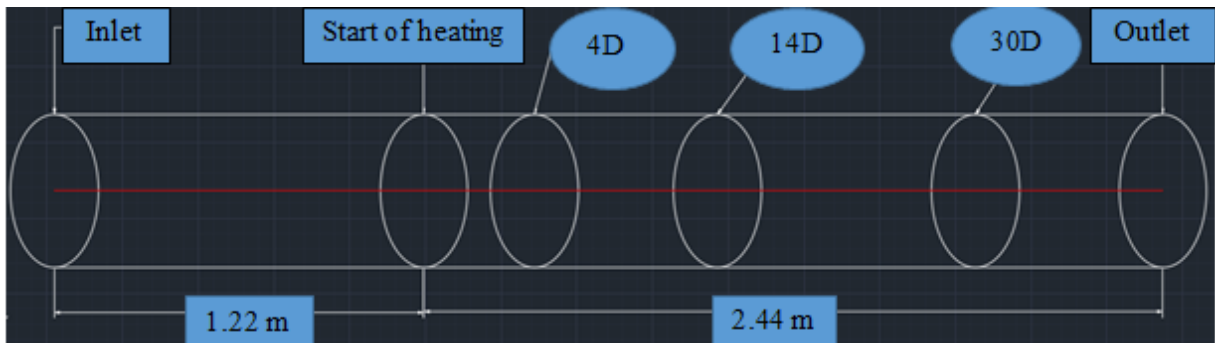
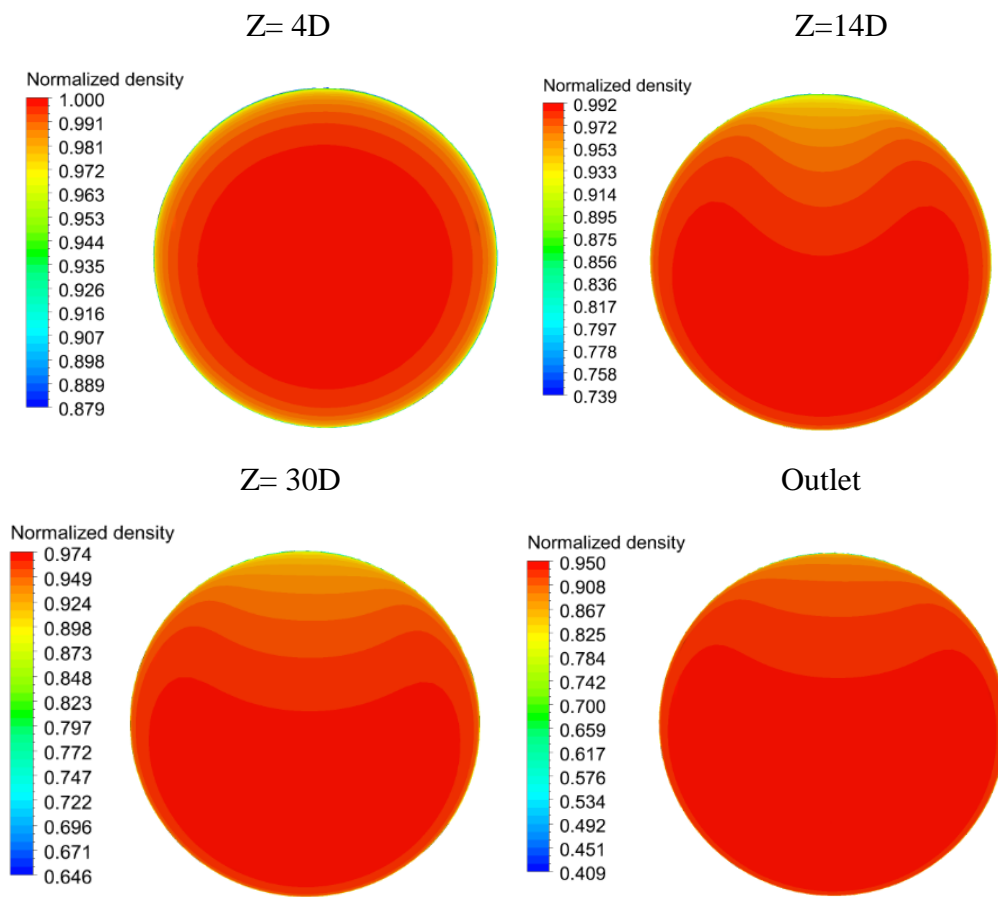


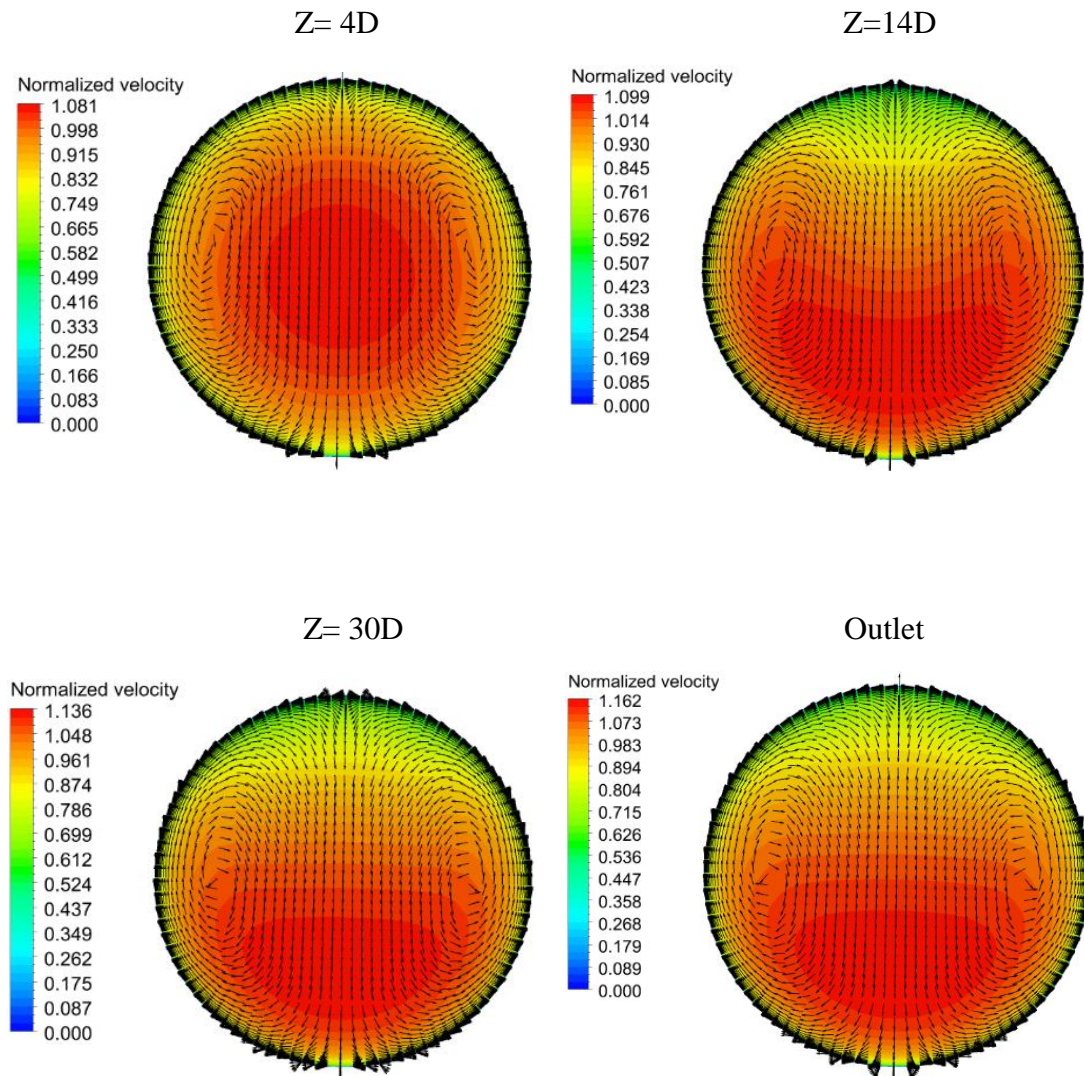
**Figure 25.** Flow domain and cross sections conditions

In test 1.2 shown by figure 26 the normalized density and velocity magnitude vectors on y-z plane are presented, consisting  $\text{CO}_2$  flows through the pipe with inlet temperature  $15.4^\circ\text{C}$  at pressure  $7.59\text{ MPa}$  and heat flux  $15.1\text{ kW/m}^2$ . It is observed clearly that at the inlet, the density contour shows the symmetric density profile for flow in heated region. The inlet temperature is uniform. The sharper temperature gradient near the wall produced due to heat addition, leads to strong  $\text{CO}_2$  density changes. Therefore, strong buoyancy force is created. The heated  $\text{CO}_2$  with higher velocity magnitude pushes upward due to buoyant force and impelled

secondary flows appeared in 14D, 30D and out let cross sections. By increasing temperature, the sharp changes of  $\text{SCO}_2$  properties happened close to the critical point, that is why the stronger vortexes or circulations shown in velocity contours are created near the wall. The secondary flow accumulated in top region of tube and it gets larger along the pipe. The maximum velocity appears in bottom region due to transferring the momentum to fluids in bottom part.



**Test 1.2.** Normalized density  $\rho/\rho_{in}$



**Test 1.2.** Normalized velocity  $U/U_{in}$

**Figure 26.** Velocity and density contours of numerical results in 1.2 test condition

Comparing density contours in appendix shows that the range of normalized density in CFD case 2.1 and 3.1 (with rather the same amount of mass flow rate and heat flux) are very similar from cross section 4D to outlet. Induce of second flow shows the similar impact on velocity value of top and bottom walls from 14D section onward in CFD case 2.1 and 3.1. Following, both normalized density and normalized velocity ranges in CFD case 1.1 and 1.2 are rather similar. In fact, in CFD cases with higher amount of mass flow rate or heat flux (Case 1.1 and

1.2) with constant pressure, the density and velocity changes are rather sharper near the critical point than CFD cases with lower amount of heat flux or mass flow rate (Case 2.1 and 3.1).

## **12 CONCLUSION**

The thermophysical properties of  $\text{SCO}_2$ , near critical point in large horizontal tube have been investigated numerically. Heat transfer and friction factor characteristics inside the tube were analysed. The numerical simulation has been examined with different turbulence models and the best approach was selected through comparing CFD and experimental results.

### **12.1 Summary of investigated model**

In the present numerical research, the unique behaviours of  $\text{CO}_2$  thermophysical characteristics near critical point in supercritical heat exchanger with considering turbulent flow have been studied. The specific focus areas were friction factor coefficient, heat transfer coefficient and temperature changes alongside the horizontal pipe. To determine thermo physical properties of  $\text{CO}_2$ , RGP table was used as real gas look up table of properties to define material and coupled with CFX solver. Moreover, the RGP dependency test has been studied to show no dependency of wall temperature to the table resolution. Mesh dependency test has done and it was shown that by increasing the structured mesh around 1300000 cells, wall temperature does not change. Near the walls, cell sizes were quite small to achieve  $y^+ < 1$ . The numerical investigation used for pipe with 22.14 mm diameter was based on 3D steady state turbulence flow models. The experimental data in this research was according to Adebisi & Hall (1976). Considering, temperature distribution validation of four turbulence models based on CFD simulation, against experimental data, the best match was selected as a default turbulence model of current investigation. Therefore, all numerical simulations were calculated with  $k-\omega$  SST turbulence model. For checking convergence, different criteria were observed such as energy, mass and momentum imbalance approached to constant zero value. Also, the observed RMS for mass and momentum was less than  $10^{-5}$  in all tests.

## 12.2 Summary of Results and validations

Numerical outcomes of simulation are summarized based on following points:

- In all four tests, temperature distribution tended to increase in both top and bottom wall uniformly and due to buoyancy effect the top wall has higher temperature than bottom wall. The highest temperature difference between top and bottom wall, which made stronger secondary flow, was related to test 1.2 with highest heat flux  $q=15100 \text{ W/m}^2$  compared to other tests.
- It can be seen that in all tests heat transfer coefficient in bottom wall was enhanced due to buoyancy force.
- Friction factor coefficients in bottom walls were higher than top wall due to higher shear stress on bottom surface as a result of applied buoyancy force.
- The averaged friction factor of the adiabatic part of the pipe has been calculated and compared with average friction factor of heating wall. It can be noticed that, by increasing the heat flux, averaged friction factor value faced bigger change from adiabatic to heated part.
- The average friction factor coefficient validated against 12 different friction factor correlations. It was observed, in the range of operating Reynolds number, the predicted friction factor coefficients used by Blasius, Lee, Morrison and Wilcox 1995 correlations had the best agreement with CFD results. To consider the effect of tube diameter on friction factor coefficient, Dang-Hihara (Dang & Hihara,2004) experimental data applied, with the same operating conditions but with one tenth tube diameter in the same Reynolds number range. It can be observed, the accurate agreement with Blasius R correlation.
- Following density contours, it was observed in all tests that flow in inlet sections were more uniform than downstream sections. As long as  $\text{CO}_2$  flows through the pipe, flow with higher velocity went downward and lower velocity flow went upward due to buoyancy effect. By increasing heat flux between test 1.1 and 1.2 at constant mass flow rate, temperature difference between wall and fluid increased, led to create

stronger vortices and un-uniform flow structure. In velocity profiles two vortices were seen due to existing significant convection flow created by buoyancy force. According to sharp variation of  $\text{SCO}_2$  properties near critical point, as temperature increased toward the critical point, effective flow circulations were observed near the wall.

- On account of observing the result of this study with respect to design of heat exchanger, it is highly recommended to model thermophysical properties through discretizing and calculate each point instead of considering constant properties specifically  $C_p$  and enthalpy.

### **12.3 Further work recommendation**

From engineering point of view, the essential achievement of this study was obtaining the operating range of heat exchanger, close to critical region based on accurate simulating conditions, which indicated that the common heat exchanger design methods which are based on some constant properties (especially isobaric specific heat) should be improved due to nonlinear change of the fluid properties especially isobaric specific heat along the heat exchanger. In fact, we need to investigate the design method to overcome sharp property change of real gas properties in the near critical point application in future studies.

## REFERENCES

Adebiyi G. A. & Hall, W. B.,1976. Experimental investigation of heat transfer to supercritical pressure carbon dioxide in a horizontal pipe.*International journal of heat and mass transfer*. vol. 19, pp. 715–720.

Ahn, Y., BAE, S. J., Kim, M., Cho, S. K., Baik, E., Lee, J. I., Cha, J. E., ScienceDirect., 2015. Review of supercritical CO<sub>2</sub> power cycle technology and current status of research and development. *Nuclear engineering technology*, vol. 47, no. 6, pp. 647–661.

Ameli, A. Afzalifar, A. Turunen-Saaresti, T. Backman, J., 2018. Effects of Real Gas Model Accuracy and Operating Conditions on Supercritical CO<sub>2</sub> Compressor Performance and Flow Field. *ASME. Journal of engineering for gas turbines and power*. Vol. 140/062603-1.

Ameli, A. Turunen-saaresti, T. backman, J., 2016. Numerical investigation of the flow behaviour inside a supercritical CO<sub>2</sub> centrifugal compressor. *Turbomachinery technical conference and exposition, GT2016-57481*. Korea. pp. 1–8.

ANSYS Inc., 2006. 12.5.2 shear stress transport k- $\omega$  model. *user guide*. Canonsburg: ANSYS.

ANSYS Inc., 2009. 8.16.1 the Aungier-Redlich-Kwong Real gas mode. Release 12, Canonsburg: ANSYS. [Online document] available at:

<http://www.afs.enea.it/project/neptunius/docs/fluent/html/ug/node335.htm>

[accessed 20 August 2018]

ANSYS Inc., 2014. *Theory manual*, Release 16, Canonsburg: ANSYS.

ANSYS Inc., Chapter 4: Turbulence and near wall modeling. Release 17. [Online document], available at: [https://www.sharcnet.ca/Software/Ansys/17.0/en-us/help/cfx\\_mod/i1345898.html](https://www.sharcnet.ca/Software/Ansys/17.0/en-us/help/cfx_mod/i1345898.html)

[Accessed 1.November 2018]

Blasius, P. R. H., 1913. Das Aehnlichkeitsgesetz bei Reibungsvorgängen in Flüssigkeiten. Forschungsheft .vol.131.no:pp.131, 1-41.

Bruch,A. Bontemps,A and Colasson,S.,2009.Experimental investigation of heat transfer of supercritical carbon dioxide flowing in a cooled vertical tube. *International journal of mass and heat transfer*, vol. 52, no. 11–12, pp. 2589–2598.

Cengel,Y.A.,2008.Introduction to thermodynamics and heat transfer.,second ed.,USA:McGrow-hill companies.

Chu,X.& Laurien,E.,2016. “Flow stratification of supercritical CO<sub>2</sub> in a heated horizontal pipe. *The journal of supercritical fluids*, vol.116,no.172-189 pp.

Dang,C. & Hihara,E.,2004. In-tube cooling heat transfer of supercritical carbon dioxide . Part 1 . Experimental measurement. *International journal of refrigeration*,vol. 27, pp. 736–747, 2004.

Dostal,V., Driscoll, M. J. , Hejzlar,. P., 2004. Advanced Nuclear Power Technology Program. A Supercritical Carbon Dioxide Cycle for Next Generation Nuclear Reactors.Doctoral thesis.MIT University.

Fang,X., Bullard, C.W., Hrnjak P.S.,2001. Heat transfer and pressure drop of gacooler.*Ashrae transactions*,vol.107.no PP:1-17.

Fatima,R.,2010.Numerical investigation of thermal hydraulic behaviour of supercritical carbon dioxide in compact heat exchangers. Master thesis, Texas A&M university.

Feher E.G.,1968. The supercritical thermodynamic power cycle, Douglas Paper no 4348, presented to the IECEC, Miami Beach,Florida,August 13-17.

Gnielinski, V., 1976. New equations for heat and mass transfer in turbulent pipe and channel flow. *International chemical engineering*. vol.16, no: pp.359–368.

Hesselgreaves, J. E., Law, R., Reay, D., 2016, Compact heat exchangers: selection, design and operation, second edition, Joe Hayton publisher.

Incropera, F. P., Dewitt, D. P., Bergman, Lavine., 2011. Fundamentals of heat and mass transfer., seventh ed., USA: Jon Wiley & Sons, Inc.

Ishizuka, T., Kato, Y., Muto, Y., Nikitin, K., Tri, N. L., Hashimoto, H., 2005. Thermal–hydraulic characteristic of a printed circuit heat exchanger in a supercritical CO<sub>2</sub> loop. The 11<sup>th</sup> International Topical Meeting on Nuclear Reactor, Thermal–Hydraulics (NURETH-11).

Jensen, M. K., Vlakancic, A., 1999. Experimental investigation of turbulent heat transfer and fluid flow in internally finned tubes, *International journal of heat and mass transfer*, vol. 42, no: pp.1343–1351.

Jiang, P., Zhao, C., Shi, R., Chen, Y., Ambrosini, W., 2009. Experimental and numerical study of convection heat transfer of CO<sub>2</sub> at super-critical pressures during cooling in small vertical tube. *International Journal of Heat and Mass Transfer*, vol. 52, no. 21–22, pp. 4748–4756.

Kim, D. E., Kim, M. H., Eun cha, J., and Kim, S. O., 2008. Numerical investigation on thermal – hydraulic performance of new printed circuit heat exchanger model . *Journal of nuclear engineering and design*. vol. 238, pp. 3269–3276.

Kim, D. E. & Kim, M. H., 2010 . Experimental investigation of heat transfer in vertical upward and downward supercritical CO<sub>2</sub> flow in a circular tube. *International Journal of Heat and Fluid Flow*, vol. 32, no. 1, pp. 176–191.

- Kim, D. E. & Kim, M. H.,2011. Two layer heat transfer model for supercritical fluid flow in a vertical tube. *The Journal of Supercritical Fluids*, vol. 58, no. 1, pp. 15–25.
- Kim, H., Kim, H. Y., Song, J. H., and Bae, Y. Y.,2008. Heat transfer to supercritical pressure carbon dioxide flowing upward through tubes and a narrow annulus passage.*Progress in nuclear energy*, vol. 50, pp. 518–525.
- Kim,M., Pettersen,J. and Bullard, C. W.,2004. Fundamental process and system design issues in CO<sub>2</sub> vapor compression systems.*Progress in energy and combustion science*, vol. 30.
- Kim,S.Gu, Lee,J., Ahn,Y., Lee,J.I, Addad,Y., Ko,B., 2014. CFD investigation of a centrifugal compressor derived from pump technology for supercritical carbon dioxide as a working fluid. *The Journal of Supercritical Fluids*, vol. 86, pp. 160–171.
- Kim,S.G., Lee,Y., Ahn,Y., Lee,J.I.,2016. CFD aided approach to design printed circuit heat exchangers for supercritical CO<sub>2</sub> Brayton cycle application. *Annals of Nuclear Energy*, vol. 92, pp. 175–185.
- Laminar boundary layers.,2018,Chapter9:Boundary layer equations. [Online document], available at: [https://nptel.ac.in/courses/112104118/lecture-28/28-2\\_boundary\\_eq.htm](https://nptel.ac.in/courses/112104118/lecture-28/28-2_boundary_eq.htm)
- [Accessed 20 October 2018]
- Lee,H.J., Kim. H., Jang,C.,2014 .Compability of candidate structural materials in high temperature SCO<sub>2</sub> environment. *The forth international symposium-supercritical CO<sub>2</sub> power cycles* ,pp. 1–9.
- Lemmon, E.W., McLinden M.O., Friend, D.G.,2015. Thermophysical properties of fluid systems in NIST chemistry Webbook, NIST standard reference database Number 69,In:P.J. Linstrom, W.G. Mallard (ed). [Online] available at: <https://webbook.nist.gov/chemistry/fluid>.
- [Accessed 21 October 2018]

Liao,S.M, & Zhao,T.S.,2002 . Measurements of Heat Transfer Coefficients from Supercritical Carbon Dioxide Flowing in Horizontal Mini / Micro channels. *Journal of heat transfer*,Vol. 124, pp. 413-419.

Li,Z., Jiang,P., Zhao,C.,Zhang,Y.,2010. Experimental investigation of convection heat transfer of CO<sub>2</sub> at supercritical pressures in a vertical circular tube.*Experimental thermal and fluid science* , vol. 34, no. 8, pp. 1162–1171.

Lindstrom, J. D., 2005.Design and evaluation of compact heat exchangers for hybrid fuel cell and gas turbine systems.Master thesis, Montana state university.

Module 4.,2018. forced convective heat transfer. lecture 15, Thermal boundary layer flow past a flat surface. [Online document], available at:

<https://nptel.ac.in/courses/103103032/module4/lec15/3.html>

[Accessed 20 October 2018]

Monaghan, R.J.,M.A.,1953. Review and Assessment of Various Formulae for Turbulent Skin Friction in Compressible Flow.*Technical report*, CP. No.142, London: Majesty's station office.

Morrison F. A.,2013. An Introduction to fluid mechanics.first ed. New York:Cambridge University Press.

Mori,K., Imanishi,H., Tsiji,Y., Hattori,T. ,matsubara,M. ,Mochizuki,S., Inada,M. Kasiwagi,T. ,2009. Direct total skin-friction measurement of a flat plate in zero-pressure- gradient boundary layers.*Fluid dynamic research*,vol.41no, p.1-19.

Ngo,T.L., Kato,Y., Nikitin,K., Tsuzuki,N.,2006. New printed circuit heat exchanger with S-shaped fins for hot water supplier. *Experimental Thermal and fluid science* ,vol. 30, pp. 811–819.

Ngo, T. L., Kato, Y., Nikitin, K., Ishizuka, T., 2007. Heat transfer and pressure drop correlations of microchannel heat exchangers with S-shaped and zigzag fins for carbon dioxide cycles. *Experimental Thermal and fluid science*. vol. 32, pp. 560–570.

Nikitin, K., Kato, Y., and Ngo, L., 2006. Printed circuit heat exchanger thermal – hydraulic performance in supercritical CO<sub>2</sub> experimental loop. *International Journal of refrigeration*. vol. 29, pp. 807–814.

Nikuradse, J., 1950. Laws of flow in rough pipes. National advisory committee for aeronautics. *NACA Technical memorandum 1292*.

Oh H. & Son, C., 2010. New correlation to predict the heat transfer coefficient in-tube cooling of supercritical CO<sub>2</sub> in horizontal macro-tubes. *Experimental Thermal and Fluid science*. vol. 34, no. 8, pp. 1230–1241.

Pioro, I. L., Duffey, R. B. and Dumouchel, T. J., 2004. Hydraulic resistance of fluids flowing in channels at supercritical pressures ( survey ). *Nuclear engineering and design*, vol. 231, pp. 187–197.

Prandtl, L., 1926. Turbulent flow. *NACA Technical memorandum, No.435*. National advisory committee for aeronautics.

Redlitch, O. & Kwong, J.N.S., 1948. On the thermodynamics of solutions. An equation of states. Fugacities of gaseous solutions. pp. 233–244.

Saeed, M. & Kim, M.H., 2017. Thermal and hydraulic performance of SCO<sub>2</sub> PCHE with different fin configurations. *Applied thermal engineering*, vol. 127, no. August, pp. 975–985, 2017.

Samson,N.& Sidum,A.,2015. Comparative modeling of hull form resistance for three ocean going vessels using methodical series.*International journal of engineering and technology* .vol.4 no.pp.489-496.

Schlichting,H.,1979.boundary layer Theory. McGraw- hill series in mechanical engineering, Seventh ed.,Germany: University of Braunschweig.

Shah, R. K. & Sekulic, D.P.,2003 .Fundamentals of heat exchanger design.Book, New York: John Wiley & Sons, Inc.

Son.C & Park.S,2006. An experimental study on heat transfer and pressure drop characteristics of carbon dioxide during gas cooling process in a horizontal tube. *International journal of refrigeration*, vol. 29, pp. 539–546.

Song,H., 2007. Investigations of a printed circuit heat exchanger for supercritical CO<sub>2</sub> and water. Master thesis. Inha University, south Korea.

Span,R. & Wagner,W., 1996 .A New Equation of State for Carbon Dioxide Covering the fluid Region from the Triple-Point Temperature to 1100 K at Pressures up to 800 MPa. vol. 25, no. 6.

Thiwaan Rao,N., Oumer,A.N., and. Jamaludin, U. K.,2016. The Journal of Supercritical Fluids State-of-the-art on flow and heat transfer characteristics of supercritical CO<sub>2</sub> in various channels. *Journal of supercritical fluid*. vol. 116, pp. 132–147.

Tsuzuki,N., Kato,Y., Nikitin,K., Ishizuka,T.,2009. Advanced microchannel heat exchanger with S-shaped fins. *Journal of nuclear science thechnology*. vol. 46, no. 5, pp. 403–412.

Was, G. S., Ampornrat,P., Gupta,G., Teyseyre.S., and E. A.,2007. Corrosion and stress corrosion cracking in supercritical water.*Journal of nuclear materials*. vol. 371, pp. 176–201.

Wilcox,D.C,1998. Basic fluid mechanics.1<sup>st</sup> ed, USA:D C W industries,Inc.

Xu, J. , Yang, C. , Zhang, W., Sun, D.,2015. Turbulent convective heat transfer of CO<sub>2</sub> in a helical tube at near-critical pressure. *International Journal of Heat and Mass Transfer*, vol. 80, pp. 748–758.

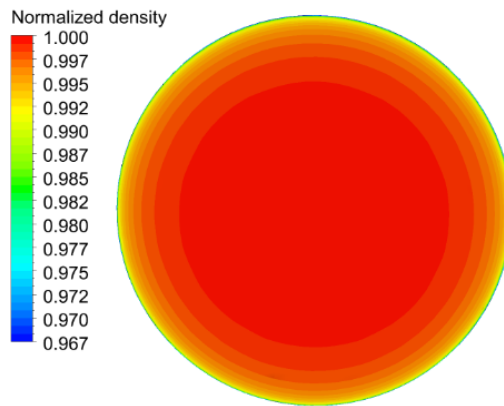
Xu,R., Luo,F., Jiang,P.,2015. Experimental research on the turbulent convection heat transfer of supercritical pressure CO<sub>2</sub> in a serpentine vertical mini tube. *International Journal of Heat and Mass Transfer.*, vol. 91, pp. 552–561.

Zhang.W, Wang,S., Li,C., Xu,J.,2015 .Mixed convective heat transfer of CO<sub>2</sub> at supercritical pressures fl owing upward through a vertical helically coiled tube. *Applied thermal engineering*, vol. 88, pp. 61–70.

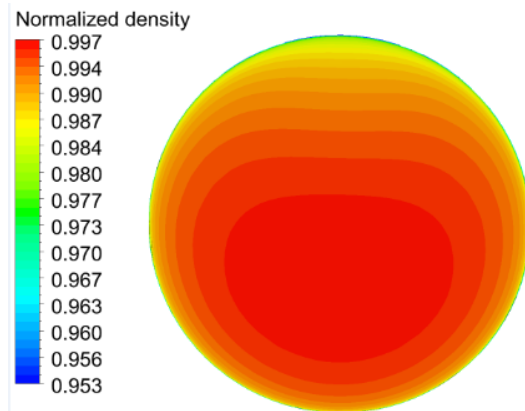
Zhang, X., 2016.Thermal-Economic optimization and structural evaluation for an advanced intermediate heat exchanger design.Master thesis, Ohio State University.

**APPENDIX:****Test 1.1**

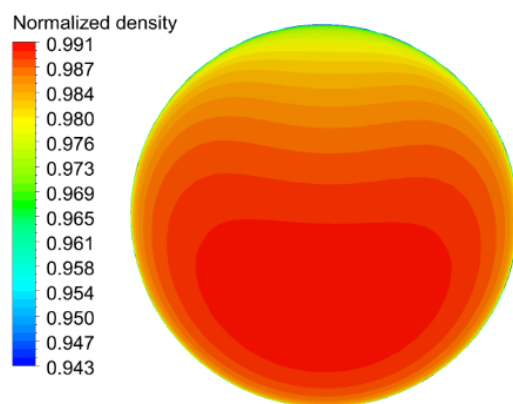
Z= 4D



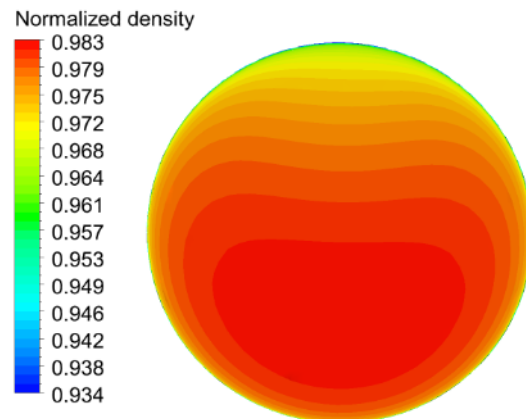
Z=14D

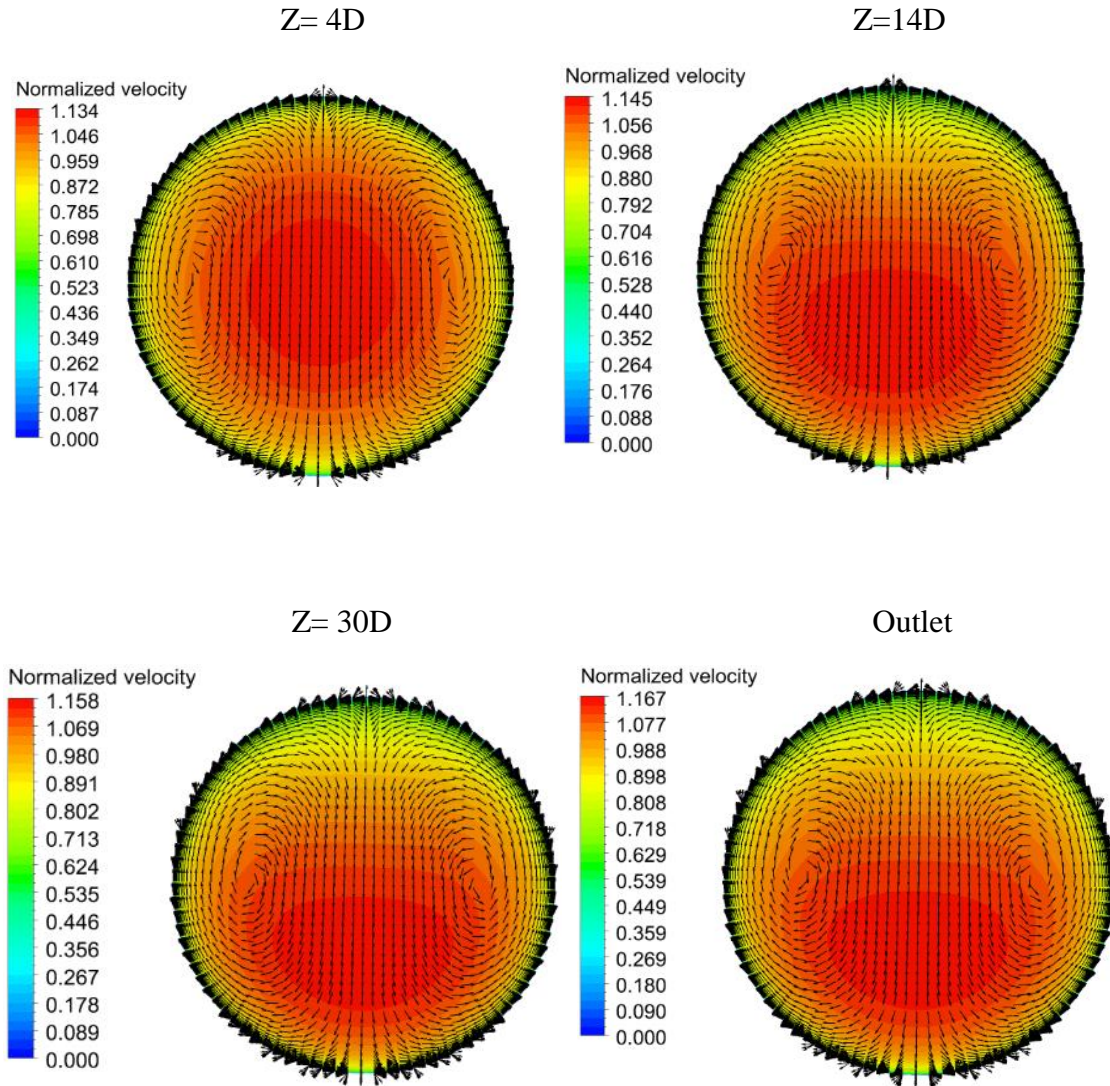


Z= 30D



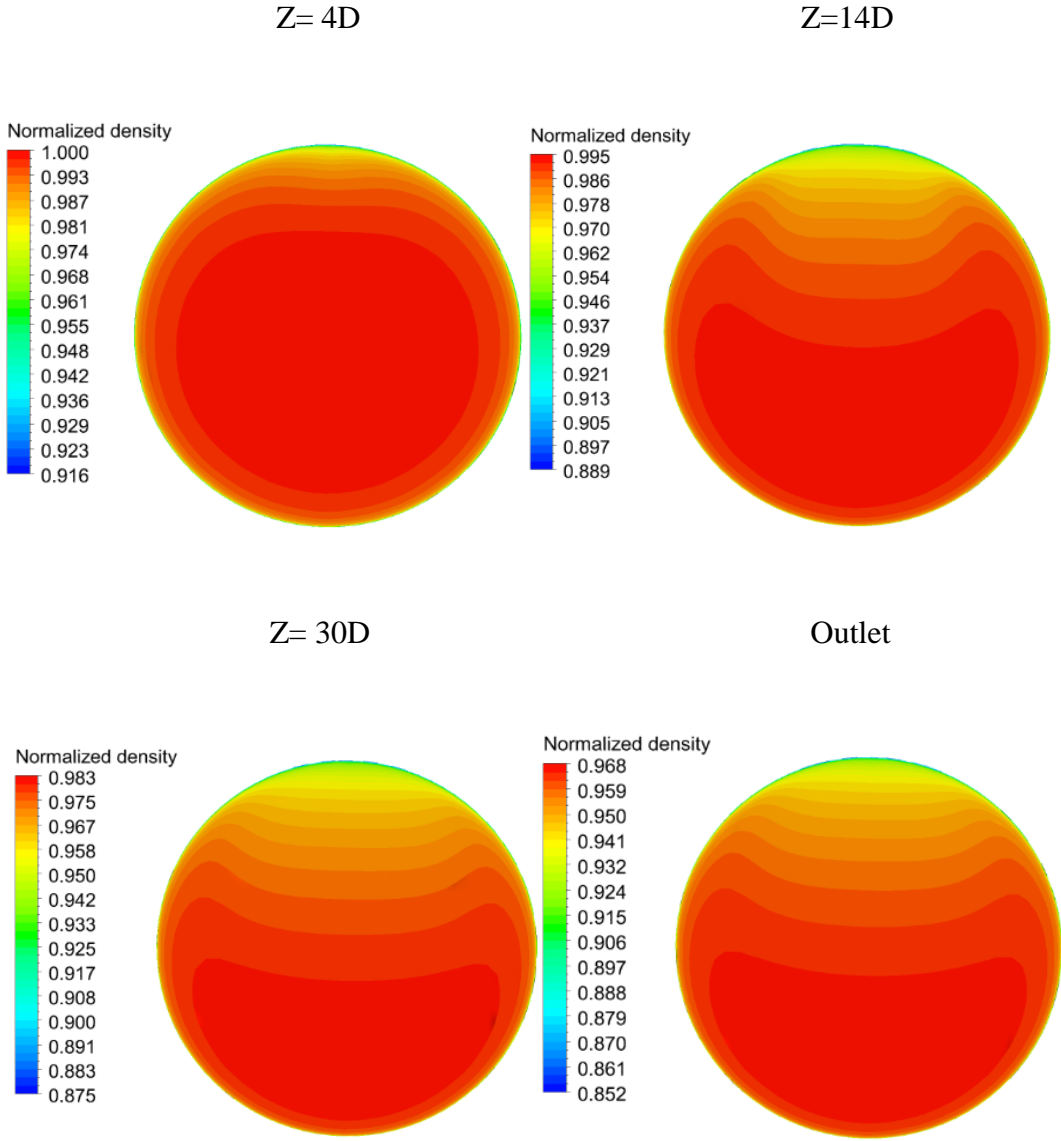
Outlet

**Test 1.1.** Normalized density  $\rho/\rho_{in}$

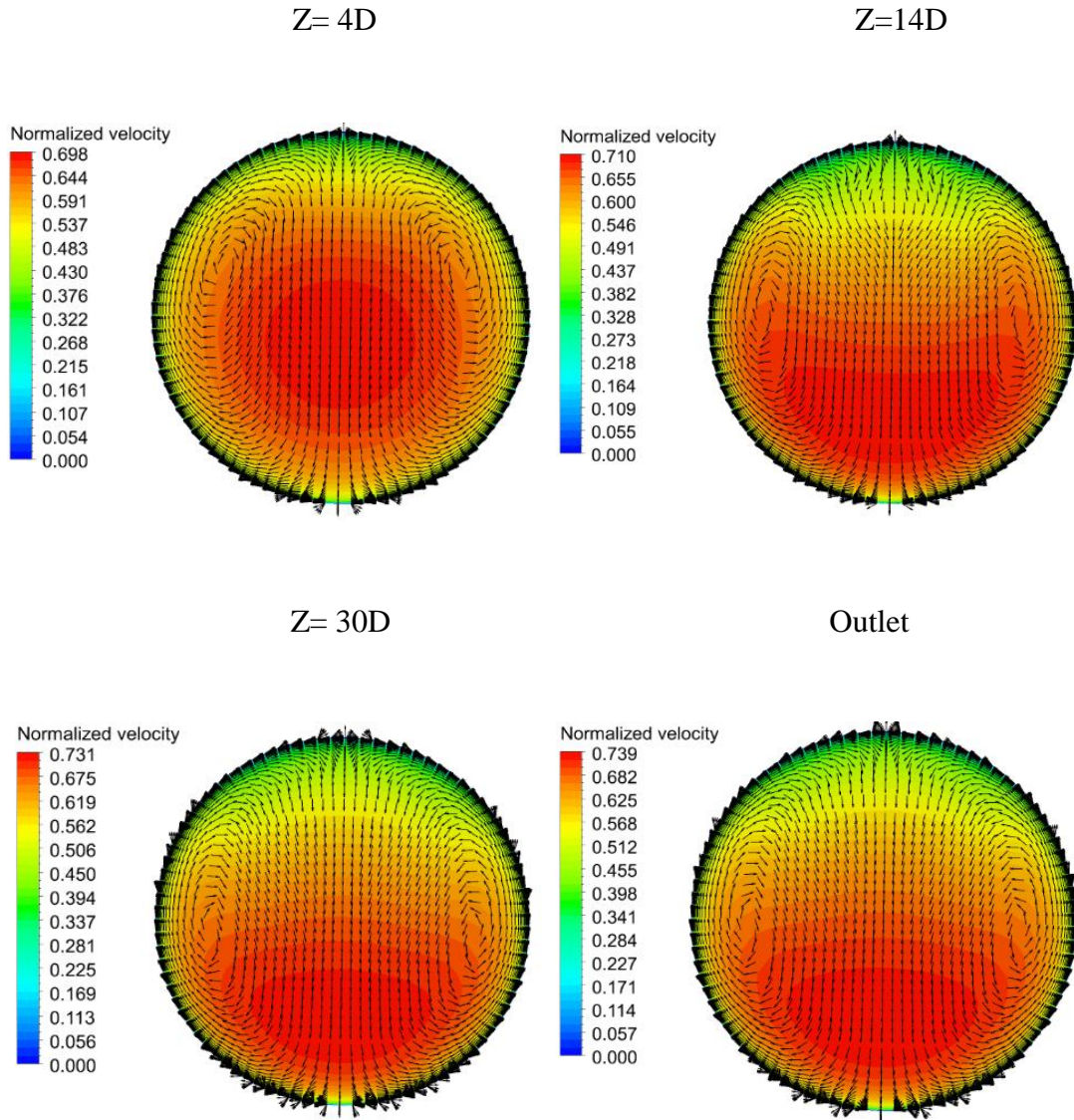


Test 1.1. Normalized velocity  $U/U_{in}$

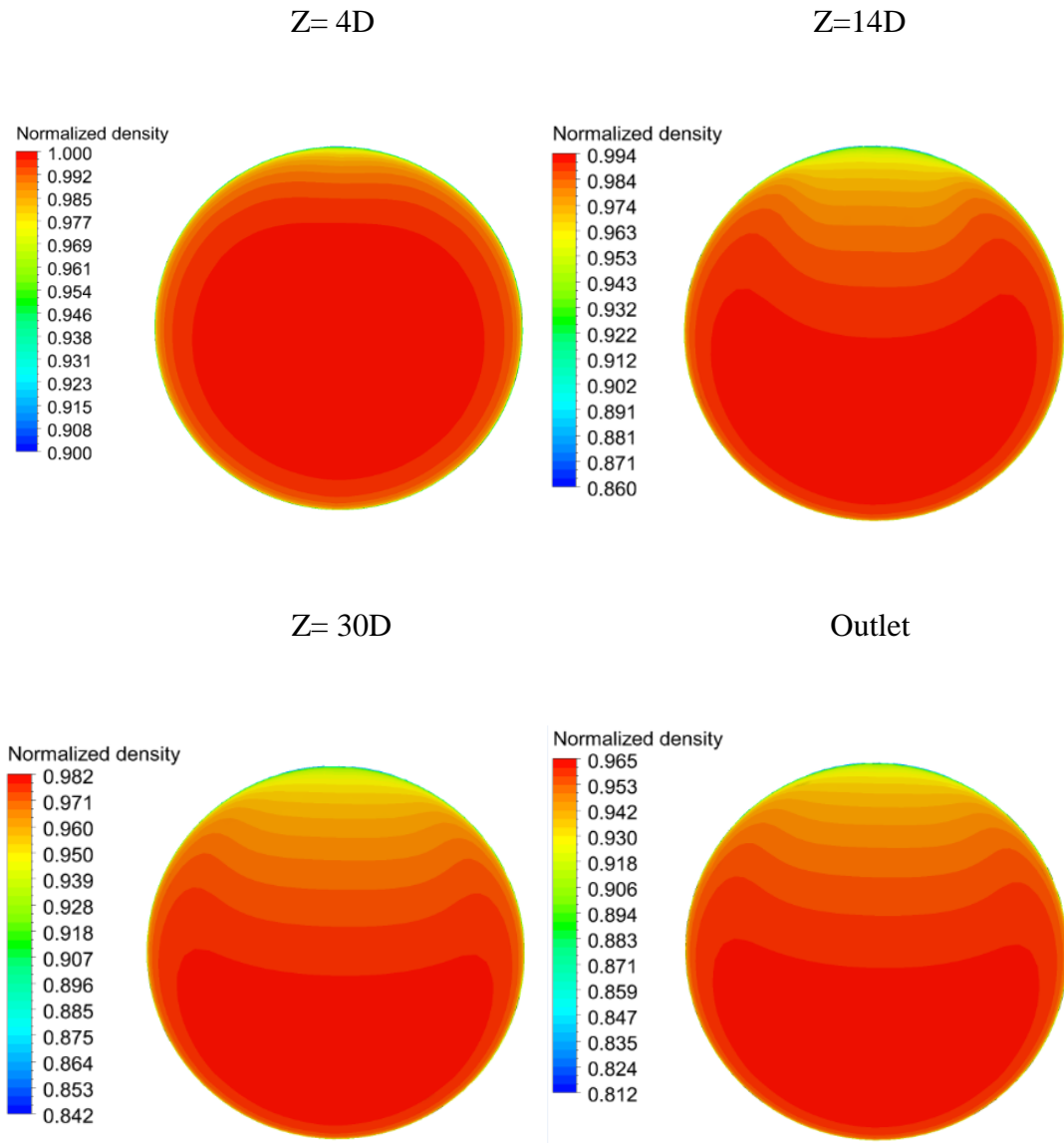
Test 2.1



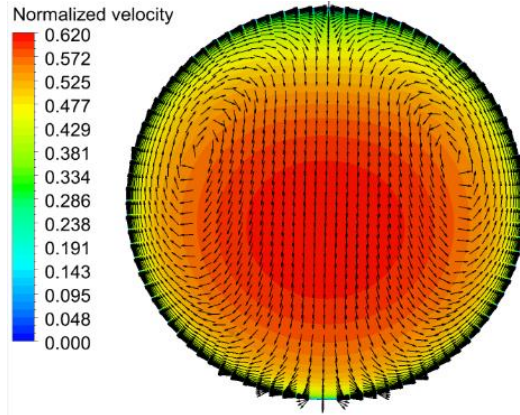
Test 2.1. Normalized density  $\rho/\rho_{in}$



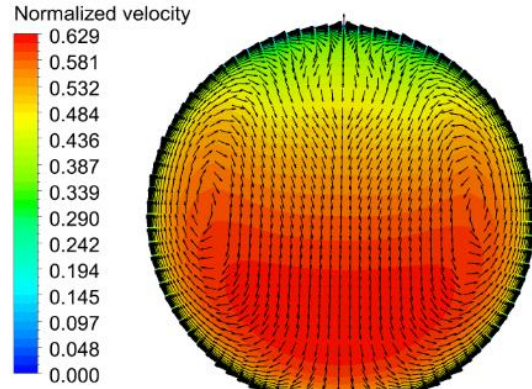
Test 2.1. Normalized velocity  $U/U_{in}$

**Test 3.1****Test 3.1.** Normalized density  $\rho/\rho_{in}$

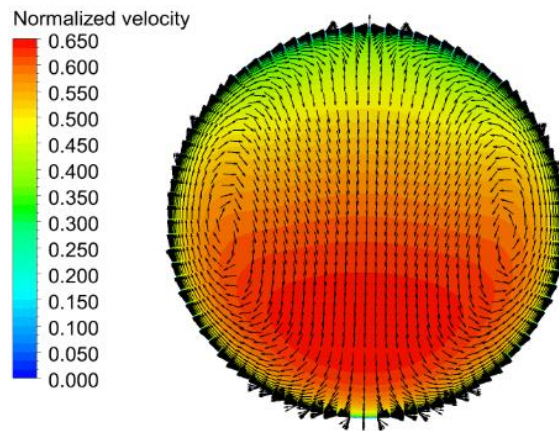
Z= 4D



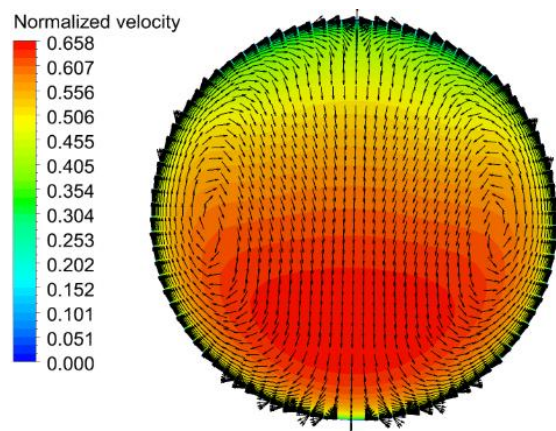
Z=14D



Z= 30D



Outlet

**Test 3.1.** Normalized velocity  $U/U_{in}$